A Review on Challenges and Successes in Atomic Scale Design of Catalysts for Electrochemical Synthesis of Hydrogen Peroxide

Samira Siahrostami,[1]* Santiago Jimenez Villegas,[1] Amir Hassan Bagherzadeh Mostaghimi,[1] Seoin Back,[2] Amir Barati Farimani,[3] Haotian Wang,[4] Kristin Aslaug Persson, [5] Joseph Montoya[5,6]

[1] Department of Chemistry, University of Calgary, 2500 University Drive NW, Calgary, Alberta, Canada T2N 1N4.
[2] Department of Chemical and Biomolecular Engineering, Sogang University, Seoul 04107, Republic of Korea
[3] Department of Mechanical Engineering, Carnegie Mellon University, Pittsburgh, Pennsylvania 15213, USA.
[4] Department of Chemical and Biomolecular Engineering, Rice University, Huston, Texas, USA
[5] Lawrence Berkeley National Laboratory, 1 Cyclotron Road, Berkeley, California, 94720, USA
[6] Toyota Research Institute, 4440 EL Camino Real, Los Altos, California, 94022, USA.

* Corresponding author: samira.siahrostami@ucalgary.ca

Abstract

Hydrogen peroxide is a valuable chemical oxidant with a wide range of applications in a variety of industrial processes, especially in water sanitization. Electrochemical synthesis of hydrogen peroxide (H_2O_2) through two-electron oxygen reduction reaction (2e-ORR) or two-electron water oxidation reaction (2e-WOR) has emerged as an appealing process for onsite production of this chemically valuable oxidant. On-site produced H_2O_2 can be applied for wastewater treatment in remote locations or any applications where H_2O_2 is needed as an oxidizing agent. This contribution studies the theoretical efforts in understanding the challenges in catalysis for electrochemical synthesis of H_2O_2 as well as providing design principles for more efficient catalyst materials.

Keywords: Electrochemical Synthesis of hydrogen peroxide; Oxygen Reduction Reaction (ORR); Water Oxidation Reaction (WOR); Computational Material Design; Density Functional Theory (DFT).

1. Introduction

Hydrogen peroxide (H_2O_2) is a benign chemical oxidant with variety of applications in industrial processes such as paper bleaching, textile, water treatment and chemical synthesis. Taking water treatment as an example, the most beneficial aspect of H_2O_2 is that it breaks down into water and oxygen after interacting with polluted water. In comparison with chlorine, the more commonly used chemical for water purification, H_2O_2 has higher oxidation potential (~1.8 V) and works twice as fast over a wider pH range. However, the cost associated with synthesis of H_2O_2 through the energy intensive, industrial anthraquinone process[1] and its transportation to the place of use hinder its widespread application in water treatment. For a similar concentration, hydrogen peroxide is more expensive than chlorine. For example, chlorine bleach usually costs $2 to $5 a gallon for 5% to 7% chlorine. However, hydrogen peroxide may cost $10 to $14 a gallon for a 7% peroxide solution. At present, the main industrial process for manufacturing H_2O_2 is the anthraquinone oxidation (AO). This process involves four main steps: (1) hydrogenation of anthraquinone with H_2 over Pd or Pt catalyst, (2) oxidation using O_2, (3) H_2O_2 extraction and (4) treatment of working solution. While AO meets the global demand of H_2O_2, it is an energy intensive multi-step process which requires large infrastructures. Further, the method is not environmentally friendly as it generates substantial waste and generated H_2O_2 requires purification, storage, and transport which negatively impacts the production cost and sustainability.[1] Thus, with all its green credentials, hydrogen peroxide would be more extensively and efficiently used if it could be made substantially and readily on-site. Direct synthesis of hydrogen peroxide (DSHP) from its constituents, H_2 and O_2, provides a straightforward pathway which has been the subject of massive research.[2–8] Palladium and its alloys are the most studied catalysts for DSHP.[3,9,10] This process has not yet been applied at industrial level due to several challenges associated with thermodynamics, explosion risk, and degradation of produced hydrogen peroxide. On the other hand, the emergence of electrochemical processes has enabled local production of this valuable chemical oxidant with high efficiency and safe operation.[11] H_2O_2 can be generated on-site from a two-electron reduction of oxygen (2e-ORR, eq. 1) and be used as an onsite oxidizing agent for water treatment.[12] This process has motivated intense research in recent years to find efficient and selective catalysts for the 2e-ORR to H_2O_2.[13–21] The

combination of computational material design and versatile synthetic methods as well as electrochemical evaluation has led to the design and discovery of the state-of-the-art Platinum and Palladium mercury alloys for this reaction.[13,14] Recently, carbon-based materials,[12,16,22,23] nitrides[21], carbides[24], sulfides[25,26], and oxides[27,28] have attracted attention as alternative cost-effective non-toxic catalysts for 2e-ORR.

$$O_2 + 2(H^+ + e^-) \rightarrow H_2O_2 \qquad E° = 0.70\ V_{RHE} \qquad (1)$$

An alternative process for onsite production of H_2O_2 and oxidize organic pollutants of water is to oxidize water in a two-electron oxidation process (2e-WOR eq. 2) in an aqueous media.[1]

$$2H_2O \rightarrow\ H_2O_2 + 2(H^+ + e^-) \qquad E° = 1.76\ V_{RHE} \qquad (2)$$

Compared to 2e-ORR, less effort has been devoted to developing catalysts for electrochemical synthesis of H_2O_2 via 2e-WOR. Mostly transition metal oxides have been examined for this reaction. Among them, some have shown high selectivity and activity and demonstrated the feasibility of this process.[29–32] Recently carbon-based materials, coupled with unique new electrode designs, have been tested and shown additional promise for this reaction.[33]

Given the growth of research interest in electrochemical H_2O_2 synthesis shown in Figure 1 (reference Scopus), and the advent of widespread adaptation of data-driven approaches to materials design, theory and computation will play an important role in the discovery of new materials for this reaction. In this review perspective we will give an overview of the emergence of computational guidance in understanding the challenges and providing solutions in designing active and selective catalysts for both 2e-ORR and 2e-WOR to produce H_2O_2. We demonstrate how simulations using the computational hydrogen electrode model reveal the Sabatier principle for H_2O_2 synthesis, explaining trends in activity towards both ORR and WOR. In this model, maximum activity is a trade-off between not too strong nor too weak adsorption energy of the adsorbates to the surface of the catalyst.[34] Furthermore, we demonstrate how simulations can

be used to construct activity volcano maps based on the Sabatier principle. This approach has proven to be powerful in predicting trends in activity across different classes of materials for many different reactions.[35–37] We emphasize that the literature includes a number of high-quality pure experimental studies in the area of 2e-ORR which have been thoroughly addressed in other review papers.[38–41] However, purely experimental studies are out of the scope of this review paper and our focus herein is on the simulation-based guidance of trends in H_2O_2 synthesis.

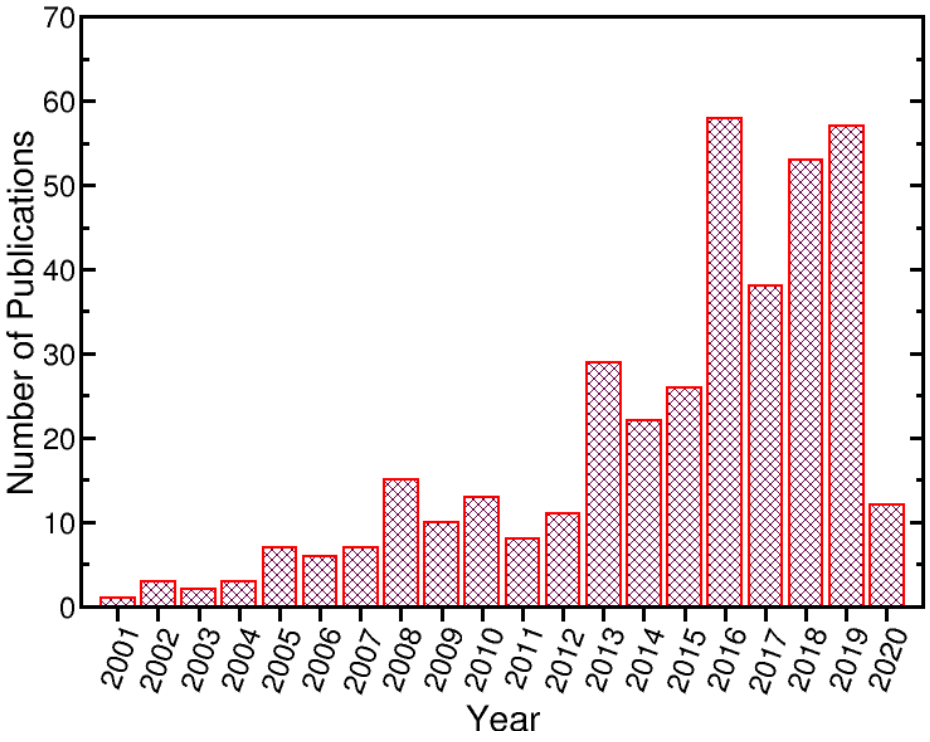

Figure 1. Number of publications for electrochemical synthesis of H_2O_2 via 2e-ORR and 2e-WOR.

2. Electrochemical Synthesis of H_2O_2 through 2e-ORR

Oxygen Reduction reaction (ORR, eq. 3, Figure 2a), where molecular oxygen is electrochemically reduced via a four-electron proton transfer to water is an emerging process of interest for chemical-to-electrical conversion technologies such as fuel cell and metal-air batteries. Both fuel cells and metal-air batteries are set to play increasingly important roles in our future sustainable energy landscape. Performance bottlenecks in zero-emission fuel-cell technologies have motivated efforts in the past three decades to discover novel catalysts and

optimize fuel-cell device design.[42–47] The four-electron ORR (4e-ORR) that occurs in a fuel cell is out of the scope of current contribution. Rather, our focus is on the 2e-ORR (eq. 4, Figure 2b) where oxygen is electrochemically reduced to H_2O_2. Similar to the 4e-ORR, this process is accompanied by generation of electrical energy.

The mechanism of 4e-ORR:

$$O_2 + 4(H^+ + e^-) \rightarrow 2H_2O \qquad E^\circ = 1.23\ V_{RHE} \tag{3}$$

$$* + O_2 + (H^+ + e^-) \rightarrow OOH^* \tag{3a}$$

$$OOH^* + (H^+ + e^-) \rightarrow H_2O + O^* \tag{3b}$$

$$O^* + (H^+ + e^-) \rightarrow OH^* \tag{3c}$$

$$OH^* + (H^+ + e^-) \rightarrow H_2O + * \tag{3d}$$

The mechanism of 2e-ORR:

$$O_2 + 2(H^+ + e^-) \rightarrow 2H_2O_2 \qquad E^\circ = 0.70\ V_{RHE} \tag{4}$$

$$* + O_2 + (H^+ + e^-) \rightarrow OOH^* \tag{4a}$$

$$OOH^* + (H^+ + e^-) \rightarrow H_2O_2 + * \tag{4b}$$

Since water is the thermodynamically favored product, the 4e-ORR competes with the 2e-ORR and the selectivity of the catalyst towards the two-electron product is an obstacle for synthesis of H_2O_2. In reality, the final product of the ORR strongly depends on the selected catalyst material. Equations (3a-d) and (4a-b) are the mechanisms for 4e- and, 2e-ORR, respectively. Figure 2c and 2d are the schematics of the two mechanisms showing that OOH* is the common intermediate between the two ORR pathways and determines the reaction product. Catalyst materials that preserve the O-O bond in the key OOH* intermediate tend to be selective towards H_2O_2. In contrast, catalysts with strong oxygen binding energies easily dissociate the O-O bond and are selective to form water as the main product. Therefore, catalysts for H_2O_2 are limited to those that bind oxygen not too strongly. In the following we show how this simple principle has led to catalyst design principles and multiple discoveries during the past few years. We first focus on pure

transition metals and then turn our focus to alloys and other classes of materials such as carbon-based materials, sulfides, and oxides.

Similarly, the adsorption strength of O_2 to the surface can be used to explain selectivity between 2e- and 4e-ORR. It has been shown that strongly bonded O_2 molecule has a parallel orientation to the surface, whereas weakly adsorbed O_2 is vertical.[48] Ab initio studies of O_2 adsorption to metal surfaces suggests that the lowest reaction barrier corresponds to a parallel orientation of oxygen followed by dissociation reaction. The perpendicular orientation of oxygen will result in higher reaction barrier for O-O bond session which results in higher 2e-ORR product.[49] These results show that as the reactivity of the surface increases it is more likely for oxygen to react with the surface through side-on mode which results in O-O bond session and following 4e-ORR pathway.

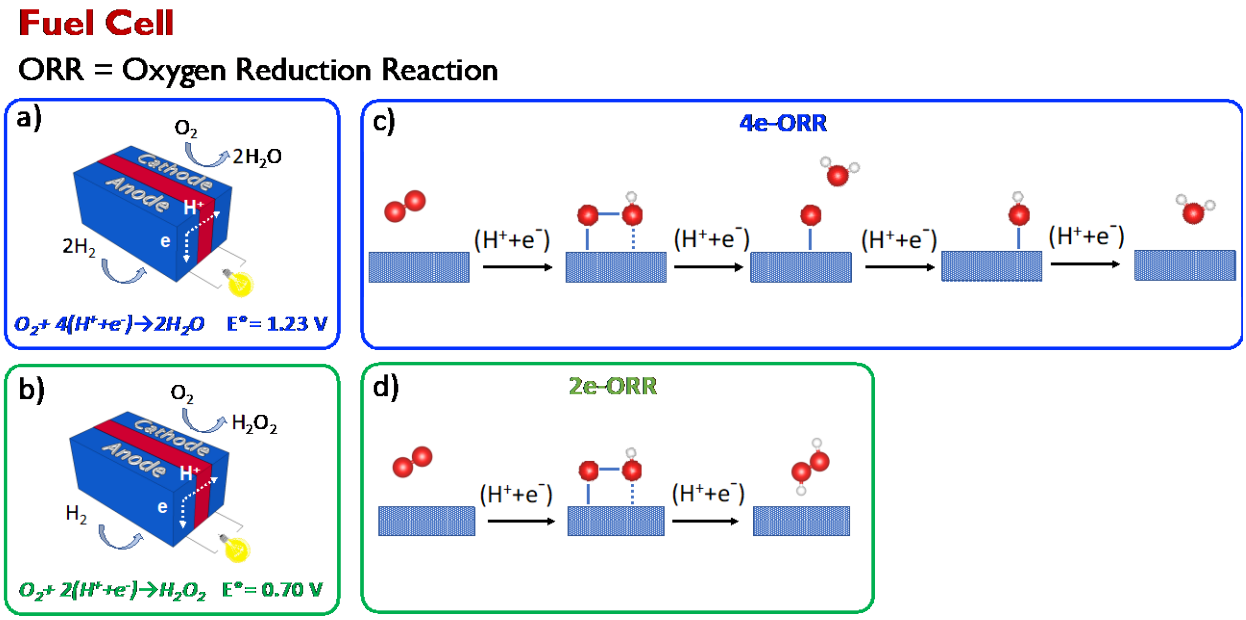

Figure 2. a) and b) are schematics of the fuel cells for the 4e-ORR that fully reduces oxygen to water as the main product and 2e-ORR which partially reduces oxygen and results in hydrogen peroxide as the major product, respectively. c) and d) are schematics of the mechanisms for 4e-ORR with water and, 2e-ORR with H_2O_2 as main products.

We note that mechanism 4(a-b) is based on acidic conditions where two coupled proton-electrons are transferred to O_2 molecule and form OOH* and subsequently H_2O_2. The 2e-ORR mechanism can also be considered for alkaline conditions;

$$O_2 + H_2O + 2e^- \rightarrow HO_2^- + OH^- \quad (5)$$

$$* + O_2 + H_2O + e^- \rightarrow OOH^* + OH^- \quad (5a)$$

$$OOH^* + e^- \rightarrow HO_2^- + * \quad (5b)$$

where, hydrogenation of oxygen (eq. 5a) is followed by the reduction of OOH* to form peroxide ion. Similar to acidic mechanism, the only involved intermediate is OOH* in basic mechanism. The difference is that the proton source in acid environment is hydronium, while it is water in base. Hence the adsorption energy of OOH* remains the best descriptor of activity in both acid and base. Adsorption energy is a surface property; therefore, it should not be affected by the proton source. Moreover, in computational modeling, everything is modeled based on RHE scale (i.e., pH= 0), which means if the active sites in the catalyst remain unchanged in acid and base, a similar trend in activity is observed among several active sties in acid and base.

2.1 Pure Metals

To model the adsorption energy of the intermediates we assume the computational hydrogen electrode (CHE) model[34], which takes the chemical potential of a proton and electron pair equivalent to that of gas-phase H_2 at potential of *U*=0 V. The effect of the electrode potential on the free energy of reaction intermediates is taken into account by shifting the electron energy by *-eU,* where *e* and *U* are the elementary charge and electrode potential, respectively. Figure 3a shows the activity volcano maps for the 2e-ORR (green) and 4e-ORR (blue) and includes the calculated limiting potential (U_L) for several transition metals as function of OH* and OOH* intermediates.[50] Dashed lines refer to the standard equilibrium potentials for 2e-ORR and 4e-ORR. The peak of the volcano graphs represents the highest activity (highest limiting potential and lowest overpotential) that can be achieved for each pathway. Shaded areas indicate the selectivity regions for H_2O (blue) or H_2O_2 (green) products. On the far right of both 2e- and 4e-volcano maps, there are catalyst materials with weak OOH* and OH* adsorption energies which indicate high selectivity for 2e-ORR and synthesis of H_2O_2. It is worth noting that OH* and OOH* intermediates follow the scaling relationship ($\Delta G_{OOH^*} = \Delta G_{OH^*} + 3.2$).[51] Therefore, both OH* or OOH* adsorption energies can be used as a descriptor of 2e and 4e-ORR activities. Figure 3a includes the analysis for both of these two descriptors. This figure shows that Au(111) weakly interacts with oxygen and therefore it is

selective for the 2e-ORR. Indeed, Au is experimentally known as the only transition metal that selectively reduces oxygen to H_2O_2.[52] However, although the selectivity is predicted, activating oxygen to form key intermediate OOH* becomes difficult due to the weak interaction of Au(111) surface with oxygen. Therefore, it costs a lot of energy to reduce oxygen to H_2O_2 on Au(111) surface. This means very low activity and high selectivity, whereas ideally both high selectivity and activity are desired. Other facets of Au such as (211) boost the activity toward 2e-ORR due to slightly stronger oxygen binding energy. However, the activity is still far below the optimum. Other transition metals such as Pt, Pd, and Ag bind OH* and OOH* strongly such that the O-O is dissociated, and they proceed via the 4e-ORR with water as the main product (Figure 3a). Figure 3b shows the free energy diagram for the 2e-ORR at the standard potential of 0.70 V. The free energy of the ideal catalyst is flat at 0.70 V which results in zero overpotential with maximum activity. Transition metals such as Pt and Pd bind OOH* intermediate too strongly such that formation of H_2O_2 becomes a bottleneck step. On the other hand on Au(211) formation of OOH* is uphill, preventing the reaction to proceed at 0.70 V.

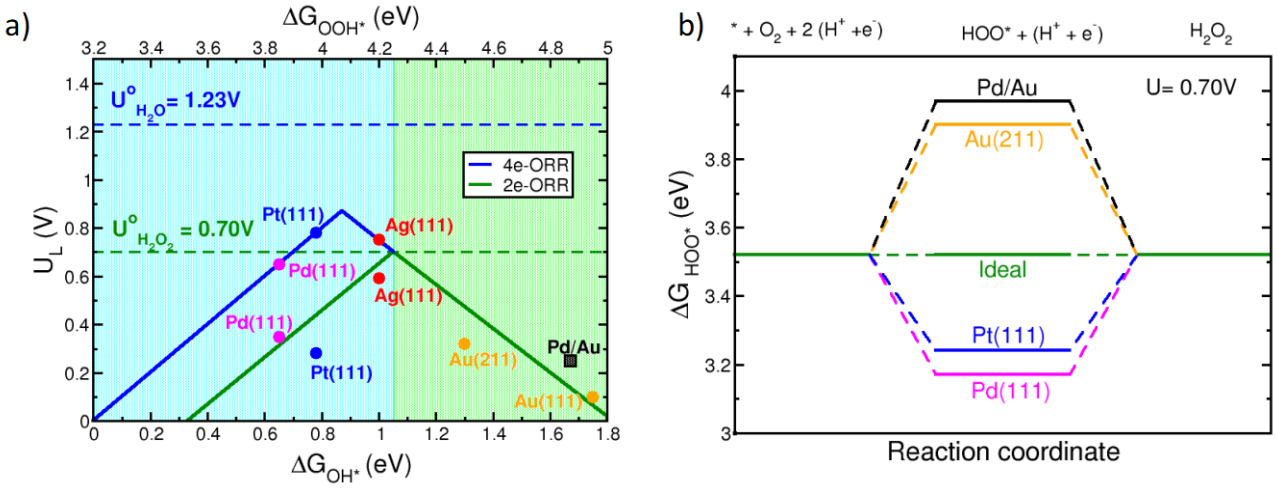

Figure 3. a) 2e-ORR (green) and 4e-ORR (blue) activity volcano plots including the activity of noble transition metals such as Pt, Pd and Au. Shaded blue and green areas represent the regions with high selectivity for H_2O and H_2O_2, respectively. b) Free energy diagram for the 2e-ORR at 0.70 V. Data for figures are adapted from Ref. [50].

2.2. Alloys

As shown in the previous section, none of the transition metals are sufficiently active and selective for 2e-ORR. In 2011, Jirkovsky, et *al*.[53], showed that active-site geometry plays a major role in determining its selectivity. They investigated alloying the surface of Au(111) with single atom sites of Pd, Pt, Rh, etc. and showed that this design helps preserving the O-O bond. As shown in Figure 3a and b, the activity of Pd/Au alloy is improved compared to Au(111) but it is almost identical to the activity of Au(211).[50]

In 2013, Siahrostami, et *al*.[13],. investigated a wide range of bulk alloys containing a single active element toward ORR (such as Pd, Pt, Rh, Ru, Ir, etc.) surrounded by an inert element (such as Hg and Au). The active element was capable of adsorbing an oxygen molecule and reducing it to OOH* but was unable to dissociate the O-O bond because the neighboring site was not prone to bond the dissociated product i.e., OH* (Figure 4a). The isolated active sites in the bulk alloys were predicted to effectively activate oxygen, therefore boosting activity and preserving selectivity towards the desired H_2O_2 product by not allowing O-O dissociation. Following these predictions, active and H_2O_2 selective Pt-Hg[13] and later Pd-Hg[14] alloys for this reaction were experimentally verified (Figure 4b). More specifically, these alloys exceeded all previous experimental activity benchmarks and exhibited 98% selectivity towards desired product. To date, they remain the most active and selective known electrocatalysts for aqueous synthesis of H_2O_2 in acidic media.

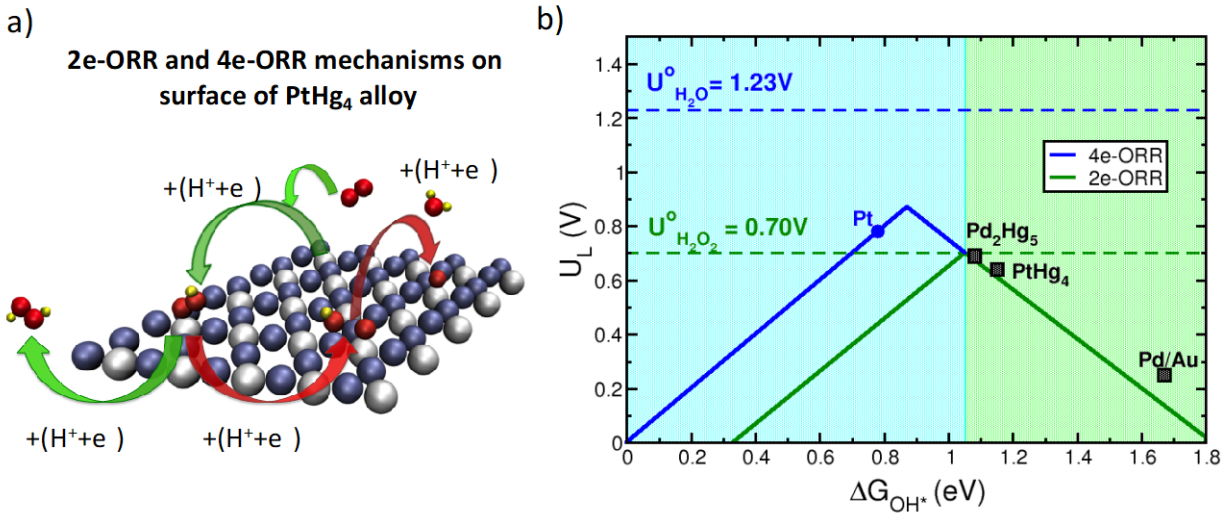

Figure 4. a) Isolated active sites in $PtHg_4$ alloy preserve O-O bond (green arrows) and maximize selectivity toward production of hydrogen peroxide, reproduced with permission from Ref. [13]. Copyright (2013, *Nat. Mater.*). b) Activity volcano plot, describing both 2e- and 4e-ORR activity plots. Shaded blue and green areas represent the regions with high selectivity for H_2O and H_2O_2, respectively.

Other alloys of mercury such as Ag-Hg and Cu-Hg have also been examined both experimentally and computationally, where Ag-Hg was shown to have an order of magnitude improvement in activity over Au.[54] Apart from alloys of mercury, other alloys have been examined and reported. Zheng et *al*.,[55] synthesized core-shell nanorods of Au-Pt-Ni using epitaxial growth and showed that lattice fringes direct the 2e-ORR pathway with 95% selectivity.

Unfortunately, the cost of noble metal-based alloys and toxicity of the state-of-the-art Pt- and Pd-Hg alloys hinder their wide-spread application. In addition to activity and selectivity, an ideal catalyst for the 2e-ORR should be cost-effective, environmentally benign, and stable under long-running electrochemical operation (Figure 5a). To this end, several alternative classes of materials have been examined. Figure 5b is a Tafel plot adapted from Ref. [38] showing the experimentally measured current density vs. onset potential for a variety of catalyst materials reported after discovery of Pt and Pd-Hg alloys. Materials with high performance are located in the top right corner of this plot with maximum current density and as close as possible potential to 0.70 V, i.e. the 2e-ORR equilibrium potential. In addition to Pt and Pd-Hg alloys, which perform well in acidic media, glassy carbon and annealed glassy carbon are shown as among the highest-performing catalysts for alkaline media in Figure 5b. Many other reports on carbon-based materials show similar performance in alkaline media, which we discuss in section 2.3.

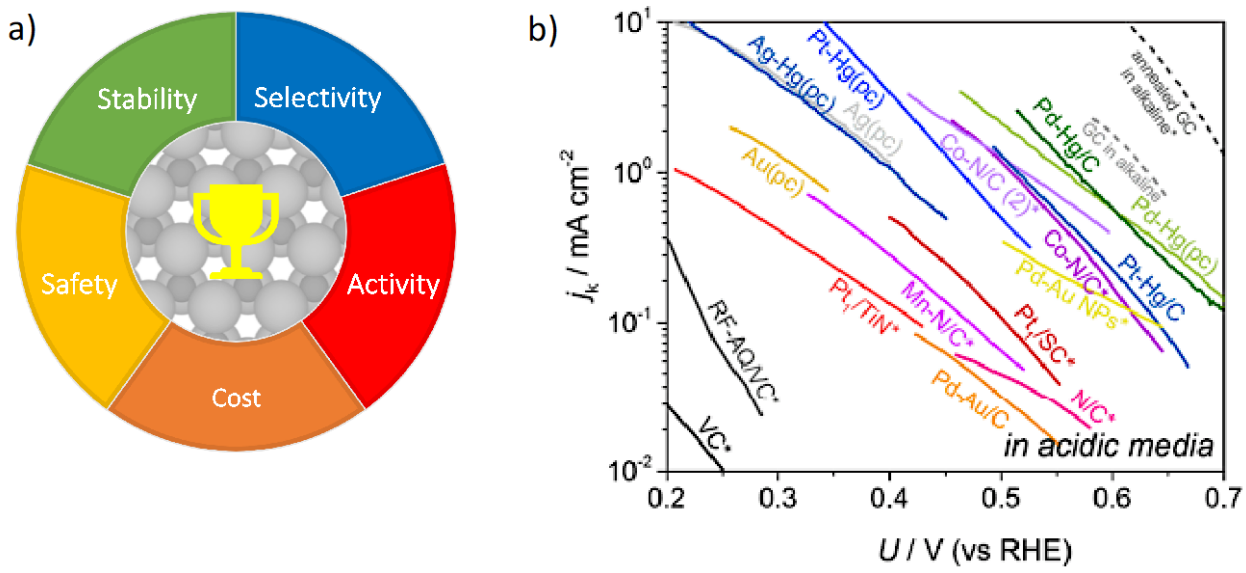

Figure 5. a) Different criteria for identifying a champion catalyst for 2e-ORR. b) Tafel plot showing the performance of several reported classes of materials for 2e-ORR, reproduced with permission from Ref. [38]. Copyright (2018, *ACS Catal.*).

2.3. Carbon-based Materials

Carbon is a key constituent of a number of non-toxic, active, and earth-abundant materials for 2e-ORR. Porous carbon materials have shown great promise in this regard owing to their high surface area, tailorable porosity, and high electronic conductivity. Hierarchical porous carbon includes various porosities from micro-/meso-/macroporous network, which can be tuned to facilitate both mass transport and activity. The electronic properties of carbon-based materials can be further tailored by introducing heteroatom or single metal dopants,[56–58] defects, and oxygen functional groups.[59] In the past few years the field of electrochemical synthesis of H_2O_2 has witnessed a significant revolution in designing carbon-based materials both experimentally and computationally.[60–65] Herein we mostly focus on highlighting literatures which have emphasized on the computational aspect as the experimental literature have been thoroughly discussed in other review articles.[38,41,66,67]

Figure 6a schematically outlines a summary of the different structural motifs used in various research efforts that may tune the activity and selectivity of carbon-based materials for 2e-ORR. Figure 6b summarizes the results of several different reports on carbon-based materials

in the context of the activity volcano shown previously. These studies can be divided into several categories; Metal and hetero-atom free carbon-based materials, oxidized carbon, carbon-based single atom catalysts, and hetero atom doping, which will be discussed separately.

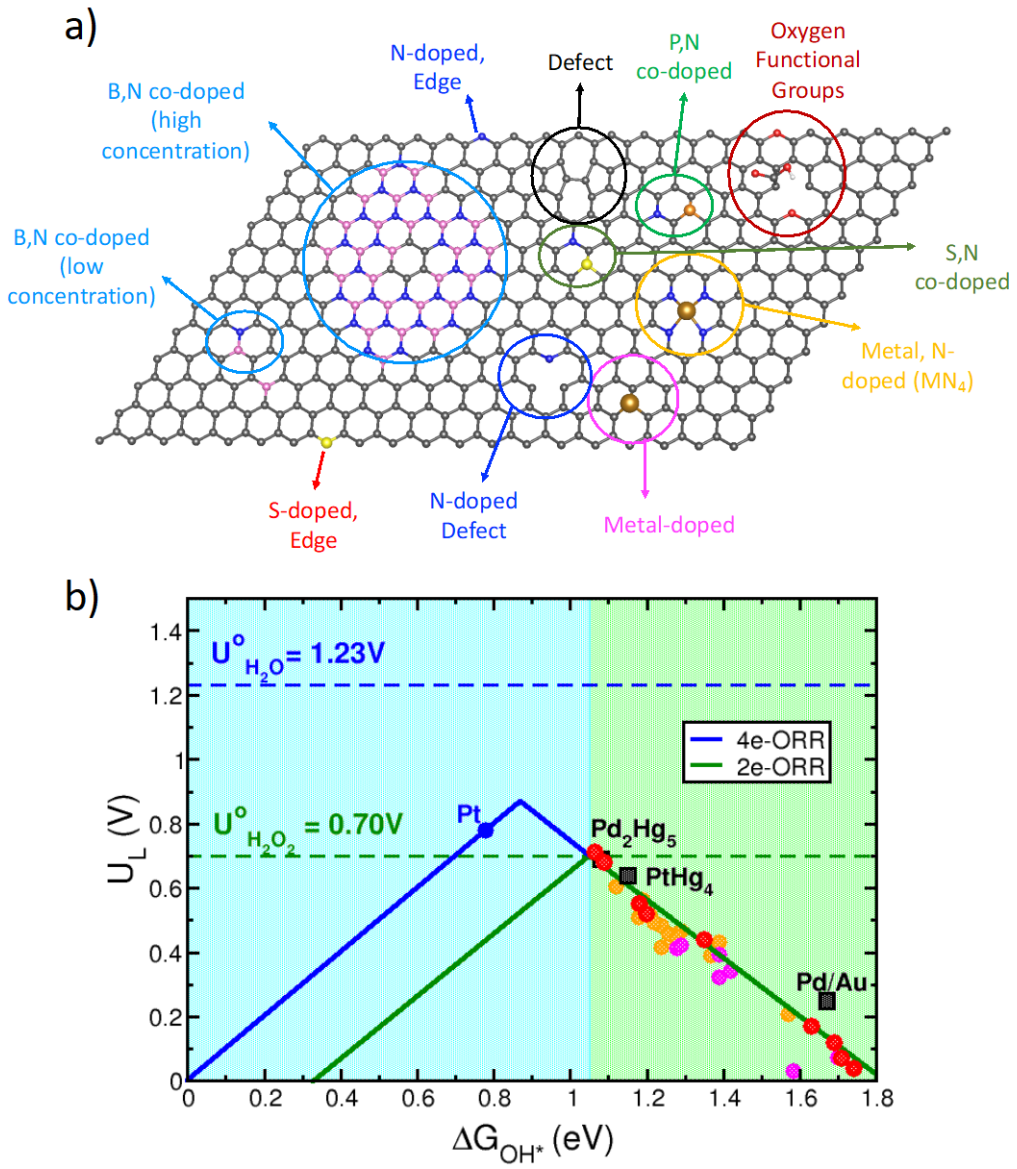

Figure 6. a) Schematic showing different efforts that have been made to tune the electronic structure of the carbon-based materials for 2e-ORR. b) Summary of the activity trends reported for variety of different carbon-based materials studied in the literature, red circles are the defect carbon (data adapted from Ref. [22]), orange: B,N co-doped carbon (data adapted from Ref. [23]), and magenta: N-doped carbon (data adapted from Ref. [44]), (values for each data point are reported in Supporting Information, Table S1).

2.3.1. Metal and hetero-atom free carbon-based materials

Carbon-based materials with no metal or heteroatom have been widely examined for ORR.[12,22,68–74] Intrinsic carbon defects (defects created by a physical or chemical method) are known to be responsible for the ORR activity. The nature of the active site has been controversial as it requires fine characterization techniques such as high-resolution transmission electron microscope (HRTEM) for direct imaging of the atomic structure and observation of different defects. Liu, et *al*.,[68] suggested that certain defects and sp^3-C bonds are the active sites. In the past years several different computational studies have been conducted to measure the activity of different possible defects.[22,70,75,76] For example, Chen et *al*.,[22] systematically examined a variety of different defects consist of pentagons, heptagons and octagons in graphene lattice with no dangling bond. These defects are known to form during synthesis procedure of different carbon samples. This study predicted that most of defects in carbon-based materials are inherently selective for production of H_2O_2 and some are very active, especially the ones with pentagons.[22]

2.3.2. Oxidized carbon

Incorporating functional groups through chemical functional design is an effective strategy to enrich the catalytic activity of carbon-based materials. In particular, oxygen functional groups have proven to significantly improve the performance of different carbon nanostructures toward 2e-ORR. A pioneer study by Lu et *al.*[16] showed that particular oxygen-containing functional groups such as ether (C-O-C) or carboxyl (-COOH) can also promote activity and selectivity for 2e-ORR in carbon materials. This work revolutionized the view about the ability of different oxygen for enhancing the 2e-ORR activity and selectivity. Many follow up works were published trying to improve selectivity and activity for 2e-ORR using different carbon nanostructures and preparation methods. The field is still growing in this direction. A recent combined experimental computational study by Han et *al*.[77] shows that quinone functional groups in the edge of carbon nanostructure exhibit high selectivity and activity for 2e-ORR.

2.3.3. Carbon-based single atoms catalysts (SACs)

Single atom catalysts SACs have emerged as an interesting catalytic system providing a unique chemistry with a great platform to explore many different reactions such as CO_2 reduction reaction, oxygen evolution reaction and oxygen reduction reaction.[78,79] Among different possible SACs, carbon-based SACs have attracted a lot of attention due to the recent advances in synthesis and characterization methods. Jiang et *al.*[17] showed that incorporating single atoms of Fe in a partially oxidized carbon substrates enhances the selectivity and activity for ORR.

A special attention has been paid to synthesizing and exploring catalytic activity of metal-nitrogen-carbon (M-N-C), in which metal is coordinated with four nitrogen atoms making a MN_4, motif also known as porphyrin in carbon substrate.[65,80,81] These systems provide a unique platform for enhancing the selectivity toward 2e-ORR while maintaining activity. A computational study by Siahrostami, et *al*.[82] in 2013 on variety of MN_4 (M = Cr, Mn, Fe, Co, Ni and Cu) embedded in graphene showed that CoN_4 has the ideal OOH* binding energy (4.23 eV) and therefore predicted to exhibit the highest activity for production of H_2O_2 among other MN_4 motifs. The recent experimental techniques have enabled careful and targeted synthesis of MN_4 motifs and works demonstrated that indeed CoN_4 is and active and selective for 2e-ORR. In the following we overview some of the recent works in this area. A combined experimental-computational study by Sun et *al.*,[65] investigated the activity and selectivity of metal-nitrogen-carbon (M-N-C) for a series of M = Mn, Fe, Co, Ni and Cu. Among these, Co-N-C was found as the most active and selective moiety for 2e-ORR both experimentally and computationally. The experimental trend in activity of different M-N-C moieties was well captured by DFT calculations and the value for the calculated limiting potential of Co-N-C was reported as 0.54 V. Similarly, Gao, et *al*.[80] calculated the activity of the same M-N-C moieties (M= Mn, Fe, Co, Ni and Cu) and showed that Co-N-C is the most active. They attributed this high activity to the end-on adsorption mode of O_2 molecule to the single metal atoms that results in optimum binding energy of OOH* and d-band center of the single metal atom.

In addition to incorporating single metal atoms in nitrogen-doped carbon, several studies have focused on adding single metal atoms in sulfur-doped carbon nanostructures to enhance the 2e-ORR selectivity and activity. Choi et *al*.[20] experimentally showed a high selectivity for atomically dispersed Pt in S-doped carbon substrate. Using DFT calculations, they investigated

several possible active sites for a single Pt atom surrounded by sulfur in graphene and reported a calculated limiting potential of 0.64 V. Tang et *al*.[83] prepared high loading of Mo-SAC with oxygen and sulfur coordination in carbon substrate and showed over 95% selectivity for 2e-ORR. DFT calculations on several Mo-O/S-C model structures revealed the critical role of coordination environment for Mo-SAC.

There are also other studies that include SACs in non-carbon-based substrates. For example, a study by Shen et *al*.,[84] shows that including single atoms of Pt in CuSx directs the selectivity towards 2e-ORR with H_2O_2 selectivity around 92%-96% in acidic electrolyte.

Apart from SACs, there are studies in the literature that focus on incorporating metal nanoparticles for tuning the electronic structure of the carbon materials and controlling the selectivity toward 2e-ORR. For example, N-doped graphitic carbon with embedded cobalt nanoparticles was examined by Lenarda et *al*.[85], and shown to produce H_2O_2 with almost 100% Faradic Efficiency at 0.5 V vs. RHE. Gan et *al*. [86] investigated the activity and selectivity of different Pt nanoparticles supported on the carbon nanotube (CNT) structure. This study demonstrated that selectivity is correlated with the size of Pt nanoparticles on the CNT such that by decreasing the size, the 2e-ORR increases. Similarly, Kim et *al*. examined activity and selectivity over a range of atomically dispersed metals (Os, Ru, Rh, Ir, and Pt) on CNT.[87] Based on this study, Pt showed the greatest selectivity towards formation of H_2O_2, while Rh showed the best activity. Selectivity was attributed to the adsorption energies of both OOH* and O*, where a proportional increase in H_2O_2 selectivity was observed with weakening of O* adsorption energy. Jung et *al*.[88] synthesized a single atom catalyst in nitrogen-doped graphene. They showed that addition of electron rich (e.g. O) or electron poor (H^+) species near the metal-N moiety results in a change of the ΔG_{OOH*}.

So far, we have shown that there are many recent studies to demonstrate the synergistic effect of the metal single atoms or nanoparticles with carbon nanostructures to enhance the performance toward 2e-ORR. However, we note that careful experimental analysis shows that many synthesis procedures for carbon-based materials will incorporate a wide range of metal impurity types and amounts.[89] These metallic impurities can significantly change the

electrochemical properties of the carbon-based materials. Therefore, careful characterization techniques are required to make sure of the absence of unanticipated metal impurities.

2.3.4. Hetero atom doping

Doping carbon-based materials with heteroatoms has also been extensively studied for boosting activity and selectivity of the 2e-ORR. Although mostly studied for 4e-ORR, N-doped carbon has been also examined for 2e-ORR.[15,62,64,90,91] A combined experimental-computational study by To, et *al*.[44], shows that N-doped into pentagonal defects drives 4e-ORR while N-doped in six member ring graphitic carbon drives the 2e-ORR. Chen et *al.*,[23] systematically examined different concentrations of boron and nitrogen co-doped in carbon. Their combined experimental and computational results revealed that hexagonal boron nitride (*h*-BN) domains formed in graphitic structure of carbon, which are energetically more favorable than individual B- and N-doped moieties, yield higher activity and selectivity toward 2e-ORR.[23] Other heteroatoms such as sulfur[92] and fluorine[93] have also been examined for the 2e-ORR. Sulfur-doped carbon has been experimentally examined by Chen et *al*.[92] which showed 70% selectivity. Computational modeling using DFT calculations showed limiting potential around 0.70 V.

Although carbon materials have shown superior activity and selectivity for 2e-ORR, their performance is limited to alkaline media. This results in difficulties in the long-term storage and transportation, since H_2O_2 is not stable under alkaline conditions. Therefore, the focus of recent studies on carbon-based materials has turned towards developing materials that are reasonably active in neutral and acidic media. The two separate studies by Lu, et *al*.[16] and Jiang et *al*.[17] demonstrated reasonable activity and selectivity for 2e-ORR under neutral pH. Very recently, Chang, et *al*.[94] showed for the first time that dispersed Pd clusters in fully oxidized carbon nanotube not only show superior activity but also high selectivity and stability under acidic conditions.

2.4. Sulfide, Oxides, Carbides, Molecular Catalysts

Apart from carbon-based materials, other classes of materials such as transition metal sulfides[25,26], oxides[27,28], and carbides[24] have been examined for 2e-ORR. Several metal-doped

RuO_2 structures have been experimentally and computationally investigated by Abbott et *al*.[27] where Ni-doped RuO_2 was shown to have selectivity and activity toward 2e-ORR with calculated limiting potentials around 0.6 V. Hybrid structures of Ni-based layered double hydroxide (Ni-LDH) dispersed on carbon nanosheets (CNS) have been shown to hinder the 4e-ORR pathway and favor the 2e-ORR. [28] Using DFT study, a synergetic relationship between the Ni-LDH and the CNS was revealed in which, through steric effects, the CNS suppressed O-O bond cleavage and production of H_2O, whereas the Ni-LDH provided defective Ni edge active sites for 2e-ORR. Based on a combined computational and experimental study, Sheng et *al*.[25] argued that structural properties of Cobalt pyrite (CoS_2) disfavour the O-O scission that is required for the 4e-ORR. They explained that the large spacing between neighbouring Co active sites prevents the two oxygens in OOH* to be adsorbed. Consequently, the O-O bond is preserved in OOH* and H_2O_2 formation is favoured. However, a study by Zhao et al.[26] shows that CoS_2 is strongly prone to oxidation under relevant pH and potential of ORR. This suggests the active phase of CoS_2 is the Co-oxy-hydroxy passivation layer on its surface. Taking several oxy-hydroxy models into account for the DFT calculations this work identifies the relevant active sites in for the 2e-ORR on CoS_2 structure. Experiments on TiC supported single atoms by Sahoo et *al*.[24] showed reasonable activity and selectivity for 2e-ORR. Trends in activity for different single atoms examined were reproduced by DFT and the limiting potential calculated for the Au doped in the TiC was reported as 0.63 V.

In addition to oxides and sulfides, advances in homogeneous catalysis are happening as well, but it is outside of the scope of this article.[95,96]

Figure 7 shows the timeline for evolving new materials for 2e-ORR in the field that are investigated with the aid of computational guidelines. For simplicity, this figure only represents the calculated limiting potentials which can be related to the activity of the material. The closer the potential to the equilibrium potential of 2e-ORR, i.e., 0.70 V the higher is its activity. We would like to emphasize once more that both activity and selectivity are important metrics in discovering new catalyst materials for 2e-ORR. Currently, there is not a well-defined computational protocol to estimate selectivity trends. However, the rotating ring disk electrode (RRDE) measurement is a proven experimental technique to measure selectivity with reasonable

accuracy. The reported numbers for selectivity are collected in Table S2 for references in Figure 7.

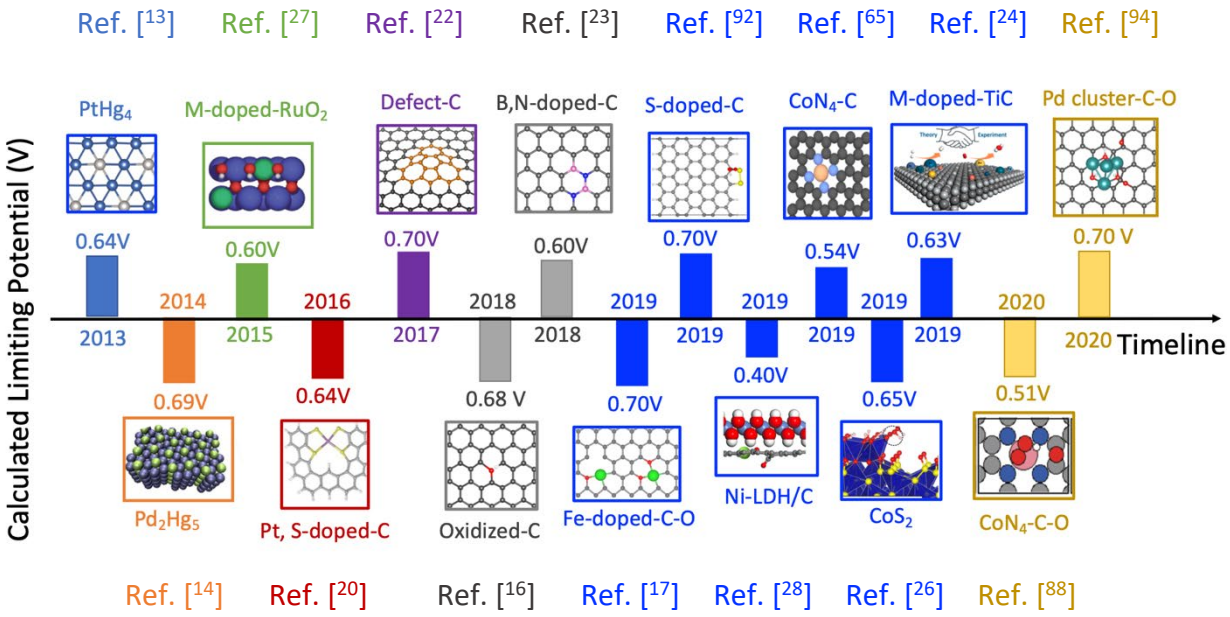

Figure 7. Timeline showing the computational reports for 2e-ORR. The bars show corresponding reported calculated limiting potentials (U_L) for the most active structure in each literature. The corresponding selectivity measured by experiment can be found in Table S2, Supporting Information.

3. Electrochemical Synthesis of H_2O_2 through water oxidation reaction

Oxidizing water is a well-known process for sustainable production of hydrogen via a four-electron water oxidation reaction (4e-WOR, eq. 6). Although the 4e-WOR (the half-oxidation reaction of water splitting) has been at the centre of attention for H_2 production,[97–105] this reaction is out of the scope of this review. Rather, our focus is on the two-electron water oxidation (2e-WOR) to produce the thermodynamically less favorable H_2O_2 (eq. 7). Apart from the 2e-WOR, a one-electron water oxidation (1e-WOR) may also occur which results in hydroxyl radical (eq. 8). Both H_2O_2 and hydroxyl radicals are powerful oxidizing agents and can be used for water disinfection. Among these, H_2O_2 is of particular interest due to its green credentials and less demanding oxidation potential (1.78 V).

The 4e-WOR:

$$2H_2O \rightarrow O_2 + 4(H^+ + e^-) \qquad E^\circ = 1.23\ V_{RHE} \qquad (6)$$

$$* + H_2O \rightarrow OH* + (H^+ + e^-) \qquad (6a)$$

$$OH* \rightarrow O* + (H^+ + e^-) \qquad (6b)$$

$$O* \rightarrow OOH* + (H^+ + e^-) \qquad (6c)$$

$$OOH* \rightarrow * + O_2 + (H^+ + e^-) \qquad (6d)$$

The 2e-WOR:

$$2H_2O \rightarrow H_2O_2 + 2(H^+ + e^-) \qquad E^\circ = 1.76\ V_{RHE} \qquad (7)$$

$$* + H_2O \rightarrow OH* + (H^+ + e^-) \qquad (7a)$$

$$* + H_2O \rightarrow OH* + (H^+ + e^-) \qquad (7b)$$

$$OH* + OH* \rightarrow H_2O_2 \qquad (7c)$$

The 1e-WOR

$$H_2O \rightarrow OH\cdot_{(aq)} + (H^+ + e^-) \qquad E^\circ = 2.38\ V_{RHE} \qquad (8)$$

$$H_2O + * \rightarrow OH* + (H^+ + e^-) \qquad (8a)$$

$$OH* \rightarrow OH\cdot_{(aq)} + * \qquad (8b)$$

Compared to the 4e-WOR, less attention has been paid to selective oxidation of water to H_2O_2 (2e-WOR) owing to the fact that it is a challenging reaction. The first experimental evidence of electrochemical oxidation of water to H_2O_2 was reported on MnO_x.[106,107] Reactive O-containing species, namely hydroxyl radicals, hydrogen peroxide, and superoxide anions have been detected at the surface of titanium dioxide under UV irradiation.[108–112] Small amounts of hydroxyl radical have been detected on the $BiVO_4$ under the visible light. [113–116] Fuku et al. reported the first successful photoelectrode system capable of producing and accumulating hydrogen peroxide.[117] In 2015, Viswanathan et al.[118] investigated the 2e-WOR using density functional theory (DFT) and showed that adsorption free energy of OH* can be used to explain the selectivity between 2e- and 4e-WOR. They also suggested OH* adsorption free energy is an appropriate descriptor for the trends in activity across different examined oxides. Later in 2017, Siahrostami, et al.,[119] addressed challenges associated with the water oxidation to hydrogen peroxide including the 1e-WOR (eq. 7) that produces OH radicals. They identified thermodynamic constraints that limit the

design of a selective and active catalyst for this reaction. Based on these, we are now capable of screening large classes of materials to identify efficient catalysts for the water oxidation to hydrogen peroxide. Herein, we briefly overview the procedure that led to identifying constraints for selectivity and activity trend across different oxide materials.

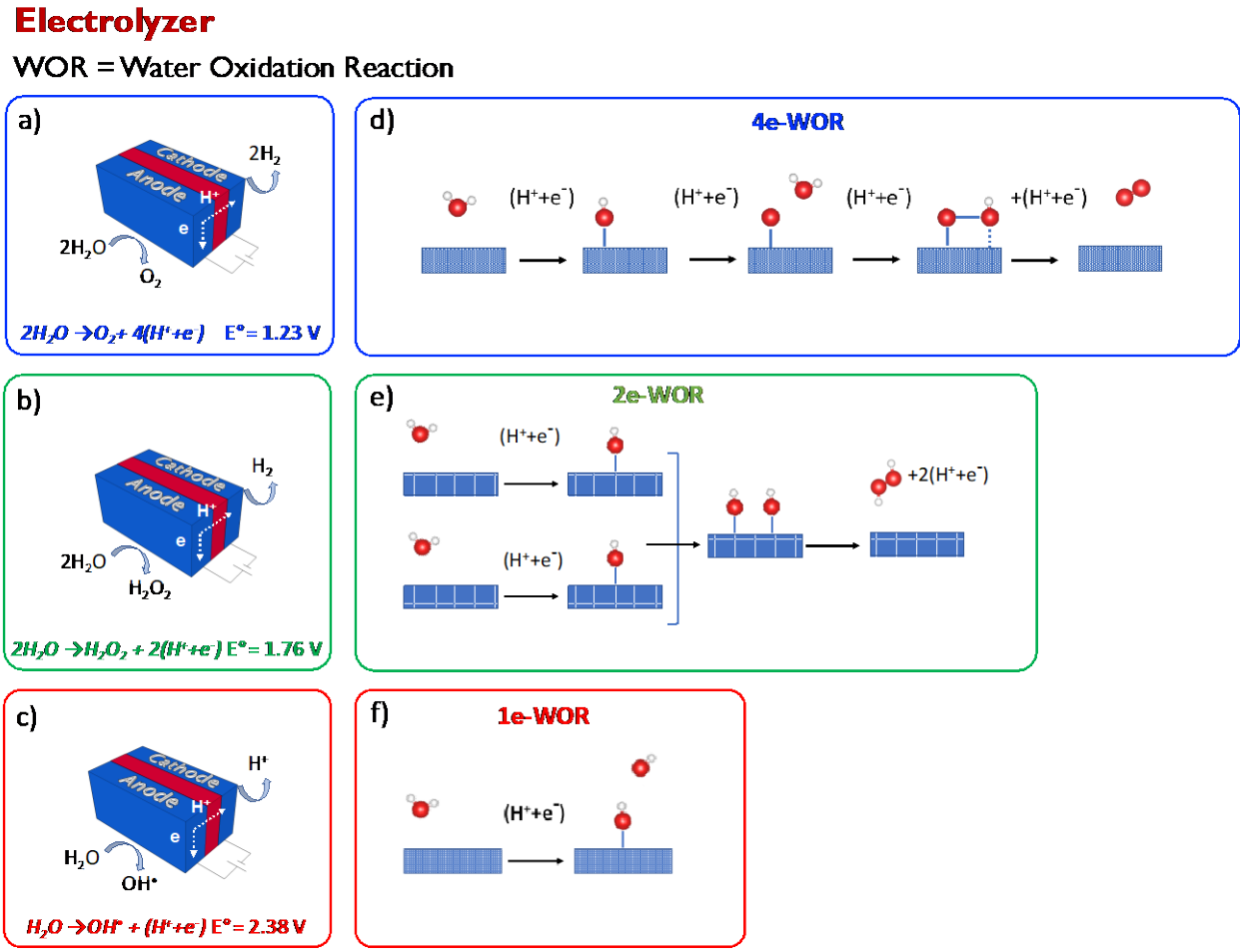

Figure 8. a) 4e-WOR that fully oxidizes water to oxygen and hydrogen as main products. b) 2e-WOR which partially oxidizes water and results in hydrogen peroxide as the major product. c) 1e-WOR, which results in OH radical. Schematics of the mechanisms for the three WORs, d) 4e-WOR, e) 2e-WOR, f) 1e-WOR.

3.1. Selectivity and Activity

The first step to capture the trends in selectivity and activity is to construct free energy diagrams for all the three WORs (Figure 8) assuming the computational hydrogen electrode (CHE) model.[34] Figure 9b shows the free energy diagram for the 2e-WOR (green solid line) to hydrogen peroxide versus the 4e-WOR (blue solid line) to oxygen on ideal catalysts at zero potential. One

of the main challenges for 2e-WOR is to prevent the 4e-WOR (eq. 5), which evolves oxygen instead of H_2O_2. This also means that once H_2O_2 forms through the 2e-WOR (eq. 6), further oxidation to O_2 (eq. 8) must be avoided.

$$H_2O_2 \rightarrow O_2 + 2(H^+ + e^-) \quad (8)$$

In order to meet these criteria and advance the reaction along the desired two-electron route, a number of constraints, in terms of binding energy of different reaction intermediates, must be imposed on the catalyst. One such constraint is that the catalyst material should be able to cleave the HO-H bond in water to ensure formation of the HO* (eq. 6a). This is an important step as the OH* is a key intermediate determining the oxidation product. Ideally, we would minimize the overpotential associated with the 2e-WOR. The overpotential for 2e-WOR is governed by the binding of a key OH* intermediate to the catalyst surface, so controlling the overpotential is a matter of tuning the free energy of OH*. The theoretical overpotential will be zero if the free energy diagram is totally flat at the equilibrium potential, i.e., 1.76 V. The H_2O_2 free energy shifts two times the equilibrium potential in response to a change in potential because it contains two electrons. Since the OH* level contains only half the number of electrons, the shift will be half as large. As a result, an OH* adsorption free energy (ΔG_{OH}) of 1.76 eV, when calculated at zero potential and relative to liquid water, will give zero overpotential. Moreover, to ensure that the four-electron path is suppressed, the catalyst must have $\Delta G_{OH} \geq 1.76\ eV$. This is due to strong OH* binding ($\Delta G_{OH} < 1.76\ eV$), which results in further oxidation and forms O* and subsequently OOH* (eq. 8) (the unfavored reaction path). This is a direct consequence of the scaling relation between the oxygenated species.[120,121] In other words, we require a catalyst with weak binding of O* and OH* not only to quench the 4e-WOR path but also to avoid further oxidation of the produced H_2O_2 (eq. 5). In terms of the free energy of adsorption, this means we require a catalyst with $\Delta G_O \geq 3.52\ eV$, and $\Delta G_{OH} \geq 1.76\ eV$ simultaneously. Simply put, a poor catalyst for 4e-WOR with high oxygen evolution overpotential has a greater chance to be a selective catalyst for the 2e-WOR.[118]

Figure 9 also represents another important constraint on the ΔG_{OH} for production of H_2O_2. This constraint is related to the free energy of the solvated OH radical (see eq. 7). The total free energy of solvated OH radical is ~2.4 eV.[122] In fact, we require a catalyst with at least $\Delta G_{OH} < 2.4\ eV$ and a simultaneously low barrier for recombining two OH* to form H_2O_2. If the OH* binding is weak and the barrier for recombination of the two OH* is high, an OH radical will be released to the solution, which results in suppression of H_2O_2 production. Note that formation of the OH radical is also beneficial for water purification, as it is able to oxidize organic pollutants. However, the production of H_2O_2 requires a lower redox potential than the OH radical.

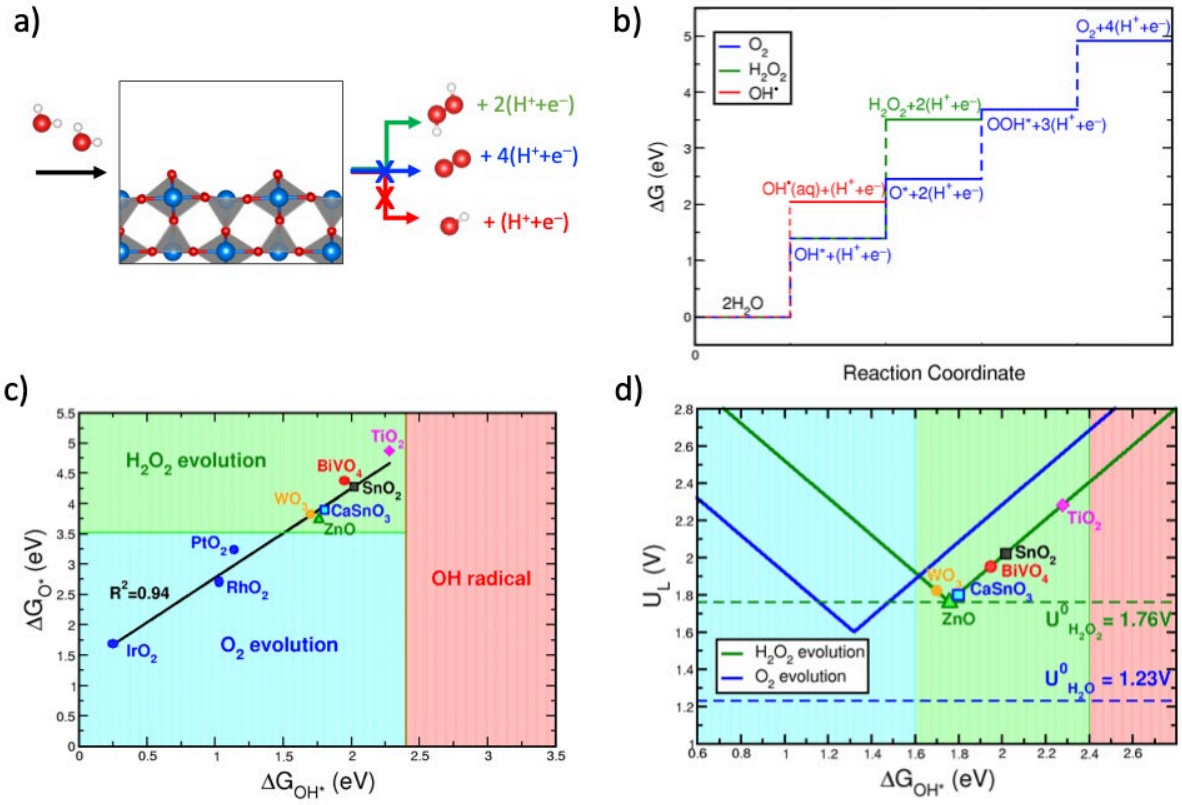

Figure 9. a) Schematics of different possible WOR pathways. b) Free energy diagram for 2e-WOR (green) vs. 4e-WOR (blue) and 1e-WOR (red). c) Product selectivity map in terms of the binding energies of O* vs. OH* showing different regions of selectivity for H_2O_2, O_2 and OH radical products. The black dashed line displays the scaling line between O* and OH* on different oxides (data adapted from Refs. [29–31,118,120,123–125]). d) Activity volcano plots for the 2e-WOR (green) and 4e-WOR (blue) showing trends in activity across different classes of materials. The corresponding equilibrium potential for each reaction has been shown in dashed lines.

The above-mentioned, purely thermodynamic constraints have been summarized in Figure 9c in terms of O* and OH* adsorption free energies in a selectivity diagram. This figure shows why PtO_2, RhO_2 and IrO_2 are known to be effective catalysts for the 4e-WOR to O_2.[118] The black dashed line in Figure 9c displays the scaling relationship between O* and OH* binding energies. Figure 9c also shows that there is a very narrow window (highlighted in green) where H_2O_2 is expected to evolve. Using these guidelines, we can rationalize the selectivity trend across a wide range of oxide materials and identify those with high selectivity for H_2O_2 product. These guidelines explain the selectivity of $BiVO_4$ for H_2O_2 production and have predicted new catalysts such as $CaSnO_3$,[31] and ZnO[29].

The analysis reported in Ref. [[118]] that applies ΔG_{OH*} as descriptor can be used to plot an activity volcano underlining the activity of the above mentioned catalyst materials towards 2e-WOR. Limiting potential, U_L, can be used as a metric of activity, defined as the lowest potential at which all the reaction steps are downhill in free energy. Figure 9d shows the calculated limiting potentials as a function of ΔG_{OH*} for both 2e-WOR and 4e-WOR. It also includes the three regions of selectivity combined with the activity volcano plot to determine the selectivity and activity of the catalyst for H_2O_2, O_2 or OH radical evolution. Several oxides, namely, TiO_2, SnO_2, $BiVO_4$, WO_3, $CaSnO_3$ and ZnO have been identified in the H_2O_2 region. The OH* binding energy of WO_3 is close to the intersection of the two volcano plots, where the two- and four-electron paths run in parallel. This agrees well with the experimental results showing that WO_3 has a low selectivity for H_2O_2 production.[30] On the other hand, $BiVO_4$ shows very high selectivity for H_2O_2 production both computationally and experimentally.[30] $CaSnO_3$[31] and ZnO[29] are very close to the peak of 2e-WOR activity volcano with nearly zero overpotential and they have experimentally been shown to be both active and selective for production of H_2O_2.

These thermodynamic guidelines can be used to search for selective and active catalysts for H_2O_2 production. We emphasize that the thermodynamic analysis has played an essential role in providing insights into the nature of active sites and guiding the design and optimization of various catalysts.[35] It has been shown that there is a close connection between the kinetic and thermodynamic formulations for oxygen electrocatalysis reactions.[126] Figure 10 applies this analysis on high-throughput computational data reported by Montoya et al.[127], that includes

around 560 different ABO_3 cubic perovskites. This report includes the adsorption energies of OH*, O*, and OOH* on all the ~500 ABO_3(100) perovskites (Figure 10a). Figure 10b shows the activity volcano map including 59 different perovskite structures with promising range of adsorption energy for O* and OH*, and potentially interesting to be explored experimentally (Table S3, Supporting Information). This descriptor-based analysis gives a straightforward method to quickly screen the most promising catalyst materials among a large data set of structures.

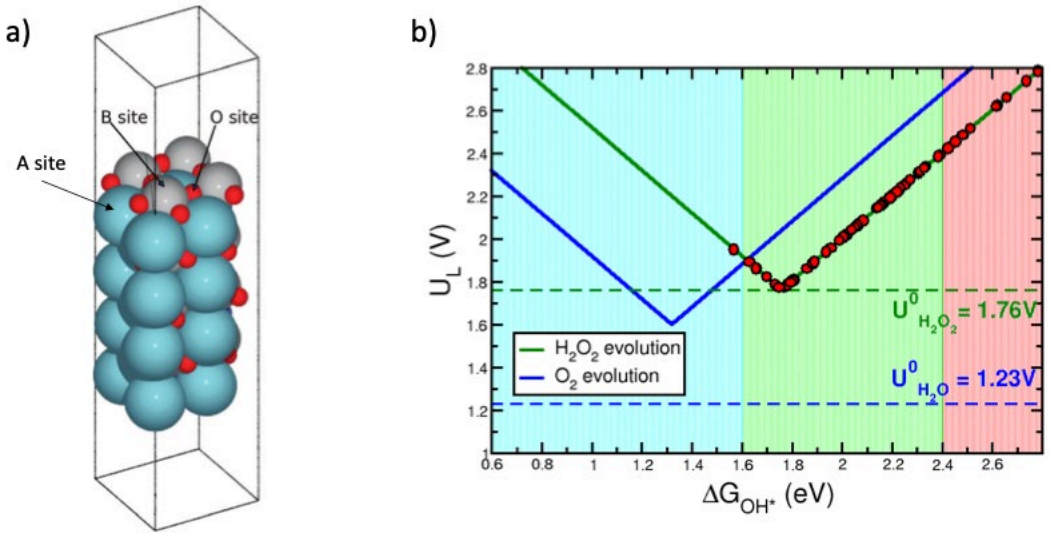

Figure 10. a) Crystal structure of ABO_3 perovskite that is used as simulation model for DFT calculations in Ref. [127]. b) Activity volcano plot summarizing the results of Ref. [127] for the 2e-WOR process in red circles. Many of the perovskites examined in this report are promising for synthesis of H_2O_2 through 2e-WOR (data in Table S3, Supporting Information).

3.2. Stability

So far, we have focused on identifying active and selective catalyst materials for 2e-WOR. However, catalyst stability is another key metric for materials for electrocatalytic synthesis of H_2O_2, and stability is strongly affected by both the extreme oxidation potential of 2e-WOR and the pH of the electrolyte. The only catalyst materials that have shown promise for this reaction are transition metal oxides, which is likely due to their partially higher tolerance of the oxidative environment. However, not all the known transition metal oxide catalysts survive long-term operation. For example, a recent study by Baek et al.,[32] shows that $BiVO_4$ is very unstable at

oxidizing potentials of >1.6 V vs. RHE, especially when illumination is used to activate $BiVO_4$ for 2e-WOR. This is consistent with theoretical predictions of solid and solution-phase ion thermochemistry[128] which predict that $BiVO_4$ should decompose under the operating potential of H_2O_2 production, i.e., ~2.0 V. into a solution-phase VO_4^- ion and a Bi_4O_7 solid. This instability is shown in the Pourbaix diagram constructed from high-throughput Materials Project data[129] (Figure 11, yellow star point). However, the stability of the $BiVO_4$ can be significantly improved by including some amount of an oxophilic element like Gadolinium.[32] Gadolinium helps stabilize the VO_4 units in the lattice of $BiVO_4$ which results in less degradation compared to bare $BiVO_4$.

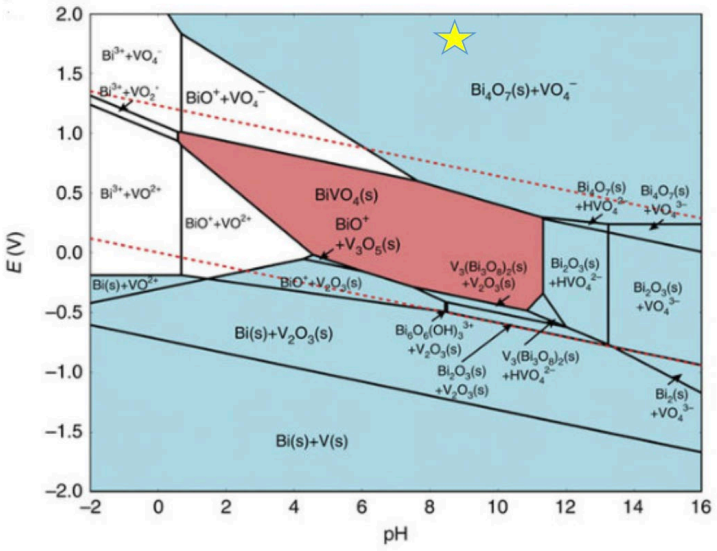

Figure 11. Pourbaix diagram of 50-50 % Bi-V system in aqueous solution, assuming a Bi ion concentration at 10^{-5} mol/kg and V ion concentration at 10^{-5} mol/kg. The upper and lower red dashed lines correspond to the equilibrium potentials for oxygen evolution reaction (OER) and hydrogen evolution reaction (HER), respectively. The cyan regions denote stable solid compounds, while the pink region is $BiVO_4$. The yellow star denotes the 2e-WOR reaction condition. Reproduced with Permission from Ref. [130]. Copyright (2016, *Nat. Commun.*).

Moving forward, there is a high demand for finding stable catalyst materials under harsh operating conditions of 2e-WOR in order to make sure they are not dissolved and therefore their catalytic activities do not degrade over time. Similar to the 2e-ORR, acidic and neutral electrolytes are highly preferred for the storage and transportation of H_2O_2. Therefore, future efforts should focus on identifying not only selective and active, but also stable oxide materials for 2e-WOR.

Pourbaix diagrams provide a useful tool that map out the compositional change for a wide range of pH and electrode potential. In other words, they represent the thermodynamic equilibrium ground states of any combination of solid and aqueous states under different pH values and potentials.[122] Software and datasets developed by the Python Material Genome (Pymatgen)[131] and Materials Project[129] enable construction of Pourbaix diagrams to evaluate electrochemical stability. More recently, capabilities for quantitative prediction of electrochemical metastability[132] and rapid analysis of many-element compositions[133] have made Pourbaix analysis of nearly every DFT-simulated material straightforward. Using these tools, one can screen a large number of oxide structures with different compositions, identify the most stable ones under desired pH and potential of the 2e-WOR. As with $BiVO_4$, one may also identify the modes of degradation depending on the decomposition product. These range from complete dissolution into solution-phase species (typically fast), partial dissolution and surface passivation (slower), or decomposition into solid-phase ground states (typically slowest under room temperature conditions).

To illustrate this analysis in practice, Figure 12 shows screening of 559 ABO_3 perovskite structures on the basis of the thermodynamic descriptor and the electrochemical stability (pH=0, 7, 14 and 2.0 V_{RHE}). A filter using the thermodynamic descriptor ($\Delta G_{OH*}, \Delta G_{O*}$) results in 59 perovskite structures with an appropriate range of O* and OH* adsorption energies. An additional stability filter using the Pourbaix diagrams generated by Pymatgen result in only 10 perovskite structures that are reasonably stable under relevant pH and potential of 2e-WOR. Note that none of the perovskites are predicted to be stable under the acidic conditions (pH=0). This highlights the importance of considering the electrochemical stability, and future research efforts should be toward the development of both active and stable catalysts.

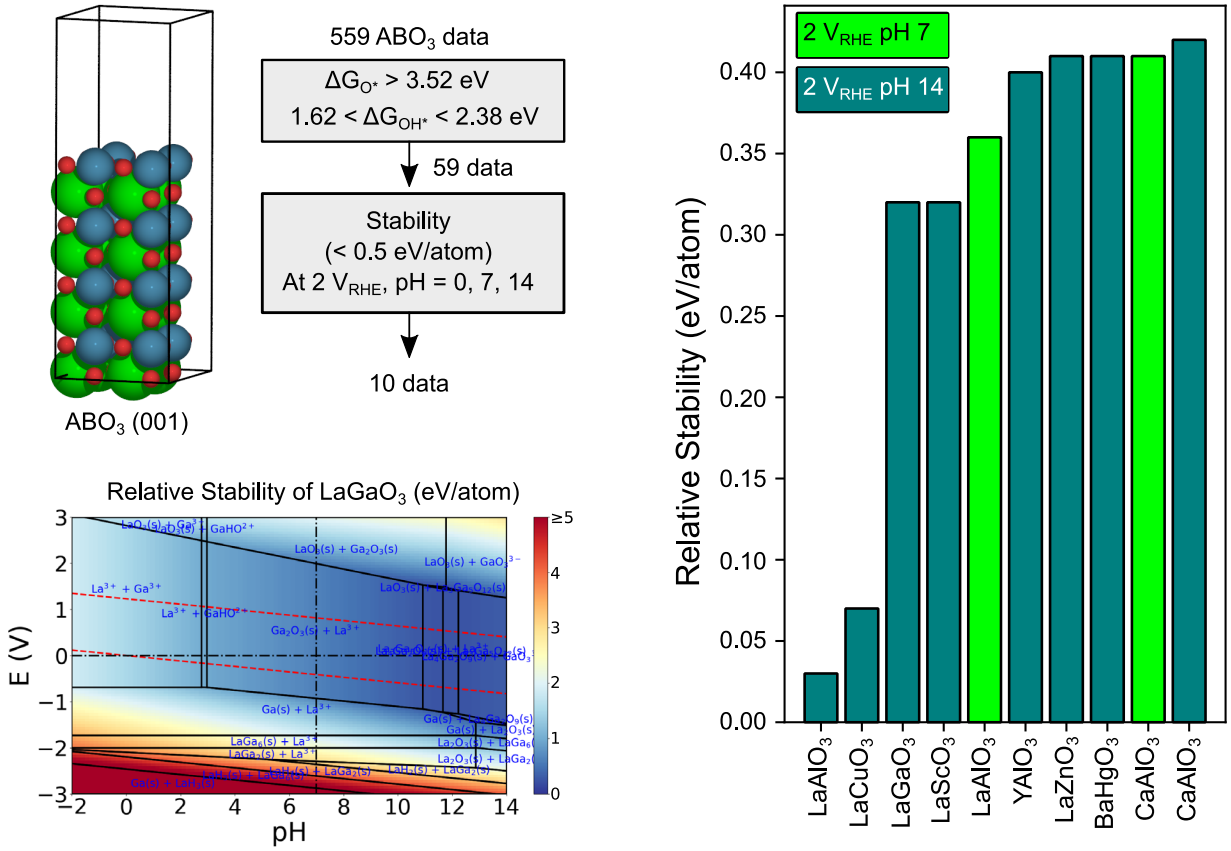

Figure 12. Screening of ABO_3 perovskites structures reported in Ref. [127]. We first collected promising candidate perovskites for 2e-WOR using the thermodynamic descriptors, followed by the stability analysis based on the Pourbaix diagram, which resulted in only 10 promising perovskites.

Summary and Perspective

Electrochemical synthesis via 2e-ORR and 2e-WOR are emerging processes of interest for onsite and sustainable production of H_2O_2. There have been numerous efforts in the literature in recent years to identify efficient, cost-effective and selective catalysts for each of these two reactions. In silico computational techniques such as density functional theory calculations have played a major role in paving the road for mechanistic understanding of these reactions and designing more efficient catalyst materials.

The 2e-ORR has been widely investigated, especially after the discovery of the state-of-the-art Pt- and Pd-Hg alloys using computational guidelines in 2013 and 2014. The main body of the research published after 2014 has been focused on the carbon-based materials, which are

attractive for the 2e-ORR due to their low cost, ease of synthesis, and facile tuning of their electronic structure. One of the drawbacks of most of the carbon-based materials is that their activity is limited to the alkaline environment in which H_2O_2 product deteriorates. This is obviously not ideal for long-term operation and storage of H_2O_2. Therefore, future research should focus on finding ways to enhance the activity of carbon-based materials in neutral and acidic environments. The work is in progress and there are already several examples of carbon materials working with excellent selectivity and activity for H_2O_2 formation.

One of the emerging areas of research in the field of electrochemical synthesis of H_2O_2 is finding strategies to avoid contamination of the product solution by extraneous ions coming from the electrolyte. This would alleviate the need for preprocessing of the produced H_2O_2. Using a porous solid electrolyte (PSE) layer instead of the liquid electrolyte is an effective approach demonstrated by Xia et *al*.,[134] to reach this goal. In this method, HOO^- and H^+ are electrochemically produced at the cathode and anode, respectively. Then these two ions are transported across the membranes and recombined within the solid electrolyte layer to produce pure H_2O_2 solutions.

Additionally, designing proper electrodes would be necessary for the 2e-ORR to increase the H_2O_2 production rate by overcoming limitations with oxygen mass transfer and low utilization efficiency of sparged oxygen. Zhang et *al*.[135] showed that a Janus electrode (JE) with asymmetric wettability structure (a hydrophobic gas storage layer and a hydrophilic catalyst layer) provides adequate oxygen supply and results in improving the H_2O_2 generation rate and oxygen utilization efficiency. Alternatively, gas diffusion electrodes (GDE) with a conjunction of a solid, liquid and gaseous interface can ideally be used to enhance oxygen mass transport and H_2O_2 production rate as demonstrated by Zhu et *al*.[136]

The 2e-WOR for electrochemical synthesis of H_2O_2 is relatively new and has recently been proven to be feasible. The first practical catalyst introduced for 2e-WOR was $BiVO_4$, which was later examined by DFT calculations and shown to be relatively active. DFT calculations have also been valuable in providing guidelines and descriptors for identifying selective and active catalysts in the materials space. However, stability under high oxidizing potentials (~ 2.0 V) for 2e-WOR poses a real challenge for long-term operation of the catalyst materials and catalytic activity

degradation. Descriptor-based analysis and new software tools like Pymatgen can predict electrochemical stability. With these techniques, one can shortlist a large number of possible structures and construct Pourbaix diagrams to evaluate electrochemical stability. Moving forward, catalyst design for the 2e-WOR reaction should follow the same protocol.

Apart from transition metal oxides, other classes of materials have been examined for the 2e-WOR. Very recently, carbon-based materials have been studied by Xia, et *al*.[33] and demonstrated to outperform previously reported transition metal oxide-based catalysts in terms of selectivity and activity. This work applies a novel approach in designing electrode interfacial engineering, whereby coating the carbon catalyst with hydrophobic polymers allowed in situ confinement of produced O_2 gas and thereby successfully tuned the water oxidation reaction pathway. Bio-inspired artificial replica is another material that have been reported for 2e-WOR. Han et *al*.[137] reported site-differentiated trinuclear manganese complexes that oxidize water to H_2O_2. These systems are interesting, although the faradic efficiency is only 15% and not competent with reported faradic efficiencies over transition metal oxides.

Acknowledgement

S.S. gratefully acknowledges the support from the University of Calgary Seed Grant and the University of Calgary's Canada First Research Excellence Fund Program, the Global Research Initiative in Sustainable Low Carbon Unconventional Resources.

Supporting Information

The data used for plotting Figures 6b, 7 and 10b are provided in the Supporting Information document.

References:

(1) Campos-Martin, J. M.; Blanco-Brieva, G.; Fierro, J. L. G. Hydrogen Peroxide Synthesis: An Outlook beyond the Anthraquinone Process. *Angew. Chem. Int. Ed. Engl.* **2006**, *45* (42), 6962–6984. https://doi.org/10.1002/anie.200503779.

(2) Plauck, A.; Stangland, E. E.; Dumesic, J. A.; Mavrikakis, M. Active Sites and Mechanisms for H2 O2 Decomposition over Pd Catalysts. *Proc. Natl. Acad. Sci. U. S. A.* **2016**, *113* (14), E1973–E1982. https://doi.org/10.1073/pnas.1602172113.

(3) Freakley, S. J.; He, Q.; Harrhy, J. H.; Lu, L.; Crole, D. A.; Morgan, D. J.; Ntainjua, E. N.; Edwards, J. K.; Carley, A. F.; Borisevich, A. Y.; Kiely, C. J.; Hutchings, G. J.; Edwards, J. K.; Hutchings, G. J.; Lunsford, J. H.; Dissanayake, D. P.; Lunsford, J. H.; Choudhary, V. R.; et al. Palladium-Tin Catalysts for the Direct Synthesis of H_2O_2 with High Selectivity. *Science* **2016**, *351* (6276), 965–968. https://doi.org/10.1126/science.aad5705.

(4) Edwards, J. K.; Freakley, S. J.; Lewis, R. J.; Pritchard, J. C.; Hutchings, G. J. Advances in the Direct Synthesis of Hydrogen Peroxide from Hydrogen and Oxygen. *Catal. Today* **2015**, *248*, 3–9. https://doi.org/10.1016/j.cattod.2014.03.011.

(5) Edwards, J. K.; Solsona, B. E.; Landon, P.; Carley, A. F.; Herzing, A.; Kiely, C. J.; Hutchings, G. J. Direct Synthesis of Hydrogen Peroxide from H2 and O2 Using TiO2-Supported Au–Pd Catalysts. *J. Catal.* **2005**, *236* (1), 69–79. https://doi.org/10.1016/j.jcat.2005.09.015.

(6) Flaherty, D. W. Direct Synthesis of H2O2 from H2 and O2 on Pd Catalysts: Current Understanding, Outstanding Questions, and Research Needs. *ACS Catal.* **2018**, *8* (2), 1520–1527. https://doi.org/10.1021/acscatal.7b04107.

(7) Li, J.; Ishihara, T.; Yoshizawa, K. Theoretical Revisit of the Direct Synthesis of H2O2 on Pd and Au@Pd Surfaces: A Comprehensive Mechanistic Study. *J. Phys. Chem. C* **2011**, *115* (51), 25359–25367. https://doi.org/10.1021/jp208118e.

(8) Rankin, R. B.; Greeley, J. Trends in Selective Hydrogen Peroxide Production on Transition Metal Surfaces from First Principles. *ACS Catal.* **2012**, *2* (12), 2664–2672. https://doi.org/10.1021/cs3003337.

(9) Edwards, J. K.; Hutchings, G. J. Palladium and Gold-Palladium Catalysts for the Direct Synthesis of Hydrogen Peroxide. *Angew. Chemie - Int. Ed.* **2008**, *47* (48), 9192–9198.

https://doi.org/10.1002/anie.200802818.

(10) Plauck, A.; Stangland, E. E.; Dumesic, J. A.; Mavrikakis, M. Active Sites and Mechanisms for H_2O_2 Decomposition over Pd Catalysts. *Proc. Natl. Acad. Sci.* **2016**, *113* (14), E1973–E1982. https://doi.org/10.1073/pnas.1602172113.

(11) Martínez-Huitle, C. A.; Ferro, S. Electrochemical Oxidation of Organic Pollutants for the Wastewater Treatment: Direct and Indirect Processes. *Chem. Soc. Rev.* **2006**, *35* (12), 1324–1340. https://doi.org/10.1039/b517632h.

(12) Chen, Z.; Chen, S.; Siahrostami, S.; Chakthranont, P.; Hahn, C.; Nordlund, D.; Dimosthenis, S.; Nørskov, J. K.; Bao, Z.; Jaramillo, T. F. Development of a Reactor with Carbon Catalysts for Modular-Scale, Low-Cost Electrochemical Generation of H_2O_2. *React. Chem. Eng.* **2017**, *2* (2), 239–245. https://doi.org/10.1039/C6RE00195E.

(13) Siahrostami, S.; Verdaguer-Casadevall, A.; Karamad, M.; Deiana, D.; Malacrida, P.; Wickman, B.; Escudero-Escribano, M.; Paoli, E. a; Frydendal, R.; Hansen, T. W.; Chorkendorff, I.; Stephens, I. E. L. S.; Stephens, I. E.; Rossmeisl, J. Enabling Direct H2O2 Production through Rational Electrocatalyst Design. *Nat. Mater.* **2013**, *12* (12), 1137–1143. https://doi.org/10.1038/nmat3795.

(14) Verdaguer-Casadevall, A.; Deiana, D.; Karamad, M.; Siahrostami, S.; Malacrida, P.; Hansen, T. W.; Rossmeisl, J.; Chorkendorff, I.; Stephens, I. E. L. Trends in the Electrochemical Synthesis of H2O2: Enhancing Activity and Selectivity by Electrocatalytic Site Engineering. *Nano Lett.* **2014**, *14* (3), 1603–1608.

(15) Fellinger, T.-P.; Hasché, F.; Strasser, P.; Antonietti, M. Mesoporous Nitrogen-Doped Carbon for the Electrocatalytic Synthesis of Hydrogen Peroxide. *J. Am. Chem. Soc.* **2012**, *134* (9), 4072–4075. https://doi.org/10.1021/ja300038p.

(16) Lu, Z.; Chen, G.; Siahrostami, S.; Chen, Z.; Liu, K.; Xie, J.; Liao, L.; Wu, T.; Lin, D.; Liu, Y.; Jaramillo, T. F.; Nørskov, J. K.; Cui, Y. High-Efficiency Oxygen Reduction to Hydrogen Peroxide Catalysed by Oxidized Carbon Materials. *Nat. Catal.* **2018**, 1–25. https://doi.org/10.1038/s41929-017-0017-x.

(17) Jiang, K.; Back, S.; Akey, A. J.; Xia, C.; Hu, Y.; Liang, W.; Schaak, D.; Stavitski, E.; Nørskov, J. K.; Siahrostami, S.; Wang, H. Highly Selective Oxygen Reduction to Hydrogen Peroxide on

Transition Metal Single Atom Coordination. *Nat. Commun.* **2019**, *10* (1), 3997. https://doi.org/10.1038/s41467-019-11992-2.

(18) Choi, C. H.; Kwon, H. C.; Yook, S.; Shin, H.; Kim, H.; Choi, M. Hydrogen Peroxide Synthesis via Enhanced Two-Electron Oxygen Reduction Pathway on Carbon-Coated Pt Surface. *J. Phys. Chem. C* **2014**, *118* (51), 30063–30070. https://doi.org/10.1021/jp5113894.

(19) Liu, Y.; Quan, X.; Fan, X.; Wang, H.; Chen, S. High-Yield Electrosynthesis of Hydrogen Peroxide from Oxygen Reduction by Hierarchically Porous Carbon. *Angew. Chemie Int. Ed.* **2015**, *54* (23), 6837–6841. https://doi.org/10.1002/anie.201502396.

(20) Choi, C. H.; Kim, M.; Kwon, H. C.; Cho, S. J.; Yun, S.; Kim, H.-T.; Mayrhofer, K. J. J.; Kim, H.; Choi, M. Tuning Selectivity of Electrochemical Reactions by Atomically Dispersed Platinum Catalyst. *Nat. Commun.* **2016**, *7*, 10922. https://doi.org/10.1038/ncomms10922.

(21) Yang, S.; Tak, Y. J.; Kim, J.; Soon, A.; Lee, H. Support Effects in Single-Atom Platinum Catalysts for Electrochemical Oxygen Reduction. *ACS Catal.* **2017**, *7* (2), 1301–1307. https://doi.org/10.1021/acscatal.6b02899.

(22) Chen, S.; Chen, Z.; Siahrostami, S.; Kim, T. R.; Nordlund, D.; Sokaras, D.; Nowak, S.; To, J. W. F.; Higgins, D.; Sinclair, R.; Nørskov, J. K.; Jaramillo, T. F.; Bao, Z. Defective Carbon-Based Materials for the Electrochemical Synthesis of Hydrogen Peroxide. *ACS Sustain. Chem. Eng.* **2018**, *6* (1), 311–317. https://doi.org/10.1021/acssuschemeng.7b02517.

(23) Chen, S.; Chen, Z.; Siahrostami, S.; Higgins, D.; Nordlund, D.; Sokaras, D.; Kim, T. R.; Liu, Y.; Yan, X.; Nilsson, E.; Sinclair, R.; Norskov, J. K.; Jaramillo, T. F.; Bao, Z. Designing Boron Nitride Islands in Carbon Materials for Efficient Electrochemical Synthesis of Hydrogen Peroxide. *J. Am. Chem. Soc.* **2018**, jacs.8b02798. https://doi.org/10.1021/jacs.8b02798.

(24) Sahoo, S. K.; Ye, Y.; Lee, S.; Park, J.; Lee, H.; Lee, J.; Han, J. W. Rational Design of TiC-Supported Single-Atom Electrocatalysts for Hydrogen Evolution and Selective Oxygen Reduction Reactions. *ACS Energy Lett.* **2019**, *4* (1), 126–132. https://doi.org/10.1021/acsenergylett.8b01942.

(25) Sheng, H.; Hermes, E. D.; Yang, X.; Ying, D.; Janes, A. N.; Li, W.; Schmidt, J. R.; Jin, S. Electrocatalytic Production of H2O2 by Selective Oxygen Reduction Using Earth-

Abundant Cobalt Pyrite (CoS2). *ACS Catal.* **2019**, *9* (9), 8433–8442. https://doi.org/10.1021/acscatal.9b02546.

(26) Zhao, W.-W.; Bothra, P.; Lu, Z.; Li, Y.; Mei, L.-P.; Liu, K.; Zhao, Z.; Chen, G.; Back, S.; Siahrostami, S.; Kulkarni, A.; Nørskov, J. K.; Bajdich, M.; Cui, Y. Improved Oxygen Reduction Reaction Activity of Nanostructured CoS2 through Electrochemical Tuning. *ACS Appl. Energy Mater.* **2019**, *2* (12), 8605–8614. https://doi.org/10.1021/acsaem.9b01527.

(27) Abbott, D. F.; Mukerjee, S.; Petrykin, V.; Bastl, Z.; Halck, N. B.; Rossmeisl, J.; Krtil, P.; Paoli, E. A.; Frydendal, R.; Hansen, T. W. Oxygen Reduction on Nanocrystalline Ruthenia – Local Structure Effects. *RSC Adv.* **2015**, *5* (2), 1235–1243. https://doi.org/10.1039/C4RA10001H.

(28) Huang, J.; Chen, J.; Fu, C.; Cai, P.; Li, Y.; Cao, L.; Liu, W.; Yu, P.; Wei, S.; Wen, Z.; Li, J. 2 D Hybrid of Ni-LDH Chips on Carbon Nanosheets as Cathode of Zinc–Air Battery for Electrocatalytic Conversion of O2 into H2O2. *ChemSusChem* **2019**, 1–9. https://doi.org/10.1002/cssc.201902429.

(29) Kelly, S. R.; Shi, X.; Back, S.; Vallez, L.; Park, S. Y.; Siahrostami, S.; Zheng, X.; Nørskov, J. K. ZnO As an Active and Selective Catalyst for Electrochemical Water Oxidation to Hydrogen Peroxide. *ACS Catal.* **2019**, *9* (5), 4593–4599. https://doi.org/10.1021/acscatal.8b04873.

(30) Shi, X.; Siahrostami, S.; Li, G.-L.; Zhang, Y.; Chakthranont, P.; Studt, F.; Jaramillo, T. F.; Zheng, X.; Nørskov, J. K. Understanding Activity Trends in Electrochemical Water Oxidation to Form Hydrogen Peroxide. *Nat. Commun.* **2017**, *8* (1), 701. https://doi.org/10.1038/s41467-017-00585-6.

(31) Park, S. Y.; Abroshan, H.; Shi, X.; Jung, H. S.; Siahrostami, S.; Zheng, X. CaSnO3: An Electrocatalyst for Two-Electron Water Oxidation Reaction to Form H2O2. *ACS Energy Lett.* **2019**, *4* (1), 352–357. https://doi.org/10.1021/acsenergylett.8b02303.

(32) Baek, J. H.; Gill, T. M.; Abroshan, H.; Park, S.; Shi, X.; Nørskov, J.; Jung, H. S.; Siahrostami, S.; Zheng, X. Selective and Efficient Gd-Doped BiVO4 Photoanode for Two-Electron Water Oxidation to H2O2. *ACS Energy Lett.* **2019**, 720–728. https://doi.org/10.1021/acsenergylett.9b00277.

(33) Xia, C.; Back, S.; Ringe, S.; Jiang, K.; Chen, F.; Sun, X.; Siahrostami, S.; Chan, K.; Wang, H. Confined Local Oxygen Gas Promotes Electrochemical Water Oxidation to Hydrogen Peroxide. *Nat. Catal.* **2020**, *3* (2), 125–134. https://doi.org/10.1038/s41929-019-0402-8.

(34) Nørskov, J. K.; Rossmeisl, J.; Logadottir, A.; Lindqvist, L.; Kitchin, J. R.; Bligaard, T.; Jónsson, H. Origin of the Overpotential for Oxygen Reduction at a Fuel-Cell Cathode. *J. Phys. Chem. B* **2004**, *108* (46), 17886–17892. https://doi.org/10.1021/jp047349j.

(35) Kulkarni, A.; Siahrostami, S.; Patel, A.; Nørskov, J. K. Understanding Catalytic Activity Trends in the Oxygen Reduction Reaction. *Chem. Rev.* **2018**, *118* (5), 2302–2312. https://doi.org/10.1021/acs.chemrev.7b00488.

(36) Greeley, J.; Jaramillo, T. F.; Bonde, J.; Chorkendorff, I. B.; Nørskov, J. K. Computational High-Throughput Screening of Electrocatalytic Materials for Hydrogen Evolution. *Nat. Mater.* **2006**, *5* (11), 909–913. https://doi.org/10.1038/nmat1752.

(37) Peterson, A. A.; Abild-Pedersen, F.; Studt, F.; Rossmeisl, J.; Nørskov, J. K. How Copper Catalyzes the Electroreduction of Carbon Dioxide into Hydrocarbon Fuels. *Energy Environ. Sci.* **2010**, *3* (9), 1311. https://doi.org/10.1039/c0ee00071j.

(38) Yang, S.; Verdaguer-Casadevall, A.; Arnarson, L.; Silvioli, L.; Čolić, V.; Frydendal, R.; Rossmeisl, J.; Chorkendorff, I.; Stephens, I. E. L. Toward the Decentralized Electrochemical Production of H2O2: A Focus on the Catalysis. *ACS Catal.* **2018**, *8* (5), 4064–4081. https://doi.org/10.1021/acscatal.8b00217.

(39) Perry, S. C.; Pangotra, D.; Vieira, L.; Csepei, L.-I.; Sieber, V.; Wang, L.; Ponce de León, C.; Walsh, F. C. Electrochemical Synthesis of Hydrogen Peroxide from Water and Oxygen. *Nat. Rev. Chem.* **2019**, *3* (7), 442–458. https://doi.org/10.1038/s41570-019-0110-6.

(40) Zhang, J.; Zhang, H.; Cheng, M. J.; Lu, Q. Tailoring the Electrochemical Production of H2O2: Strategies for the Rational Design of High-Performance Electrocatalysts. *Small* **2019**, *1902845*, 1–17. https://doi.org/10.1002/smll.201902845.

(41) Jiang, Y.; Ni, P.; Chen, C.; Lu, Y.; Yang, P.; Kong, B.; Fisher, A.; Wang, X. Selective Electrochemical H2O2 Production through Two-Electron Oxygen Electrochemistry. *Adv. Energy Mater.* **2018**, *8* (31), 17–19. https://doi.org/10.1002/aenm.201801909.

(42) Tripkovic, V.; Skulason, E.; Siahrostami, S.; Norskov, J. K.; Rossmeisl, J. The Oxygen

Reduction Reaction Mechanism on Pt(111) from Density Functional Theory Calculations. *Electrochim. Acta* **2009**, *55* (27), 7975–7981.

(43) Back, S.; Hansen, M. H.; Garrido Torres, J. A.; Zhao, Z.; Nørskov, J. K.; Siahrostami, S.; Bajdich, M. Prediction of Stable and Active (Oxy-Hydro) Oxide Nanoislands on Noble-Metal Supports for Electrochemical Oxygen Reduction Reaction. *ACS Appl. Mater. Interfaces* **2019**, *11* (2), 2006–2013. https://doi.org/10.1021/acsami.8b15428.

(44) To, J. W. F.; Ng, J. W. D.; Siahrostami, S.; Koh, A. L.; Lee, Y.; Chen, Z.; Fong, K. D.; Chen, S.; He, J.; Bae, W.-G.; Wilcox, J.; Jeong, H. Y.; Kim, K.; Studt, F.; Nørskov, J. K.; Jaramillo, T. F.; Bao, Z. High-Performance Oxygen Reduction and Evolution Carbon Catalysis: From Mechanistic Studies to Device Integration. *Nano Res.* **2017**, *10* (4), 1163–1177. https://doi.org/10.1007/s12274-016-1347-8.

(45) Higgins, D.; Wette, M.; Gibbons, B. M.; Siahrostami, S.; Hahn, C.; Escudero-Escribano, M.; García-Melchor, M.; Ulissi, Z.; Davis, R. C.; Mehta, A.; Clemens, B. M.; Nørskov, J. K.; Jaramillo, T. F. Copper Silver Thin Films with Metastable Miscibility for Oxygen Reduction Electrocatalysis in Alkaline Electrolytes. *ACS Appl. Energy Mater.* **2018**, *1*, 1990–1995. https://doi.org/10.1021/acsaem.8b00090.

(46) Greeley, J.; Stephens, I. E. L.; Bondarenko, A. S.; Johansson, T. P.; Hansen, H. A.; Jaramillo, T. F.; Rossmeisl, J.; Chorkendorff, I.; Nørskov, J. K. Alloys of Platinum and Early Transition Metals as Oxygen Reduction Electrocatalysts. *Nat. Chem.* **2009**, *1* (7), 552–556. https://doi.org/10.1038/nchem.367.

(47) Xin, H.; Holewinski, A.; Linic, S. Predictive Structure–Reactivity Models for Rapid Screening of Pt-Based Multimetallic Electrocatalysts for the Oxygen Reduction Reaction. *ACS Catal.* **2012**, *2* (1), 12–16. https://doi.org/10.1021/cs200462f.

(48) Montemore, M. M.; van Spronsen, M. A.; Madix, R. J.; Friend, C. M. O2 Activation by Metal Surfaces: Implications for Bonding and Reactivity on Heterogeneous Catalysts. *Chem. Rev.* **2018**, *118* (5), 2816–2862. https://doi.org/10.1021/acs.chemrev.7b00217.

(49) Cheng, J.; Libisch, F.; Carter, E. A. Dissociative Adsorption of O2 on Al(111): The Role of Orientational Degrees of Freedom. *J. Phys. Chem. Lett.* **2015**, *6* (9), 1661–1665. https://doi.org/10.1021/acs.jpclett.5b00597.

(50) Siahrostami, S.; Verdaguer-Casdevall, A.; Karamad, M.; Chorkendorff, I.; Stephens, I. E. L.; Rossmeisl, J. Activity and Selectivity for O2 Reduction to H2O2 on Transition Metal Surfaces. *ECS Trans.* **2013**, *58* (2), 53–62. https://doi.org/10.1149/05802.0053ecst.

(51) Koper, M. T. M. Theory of Multiple Proton–Electron Transfer Reactions and Its Implications for Electrocatalysis. *Chem. Sci.* **2013**, *4* (7), 2710. https://doi.org/10.1039/c3sc50205h.

(52) Marković, N. M.; Adić, R. R.; Vešović, V. B. Structural Effects in Electrocatalysis: Oxygen Reduction on the Gold Single Crystal Electrodes with (110) and (111) Orientations. *J. Electroanal. Chem. Interfacial Electrochem.* **1984**, *165* (1), 121–133. https://doi.org/10.1016/S0022-0728(84)80091-1.

(53) Jirkovský, J. S.; Panas, I.; Ahlberg, E.; Halasa, M.; Romani, S.; Schiffrin, D. J. Single Atom Hot-Spots at Au-Pd Nanoalloys for Electrocatalytic H2O2 Production. *J. Am. Chem. Soc.* **2011**, *133* (48), 19432–19441. https://doi.org/10.1021/ja206477z.

(54) Verdaguer-Casadevall, A.; Deiana, D.; Karamad, M.; Siahrostami, S.; Malacrida, P.; Hansen, T. W.; Rossmeisl, J.; Chorkendorff, I.; Stephens, I. E. L. Trends in the Electrochemical Synthesis of H_2O_2: Enhancing Activity and Selectivity by Electrocatalytic Site Engineering. *Nano Lett.* **2014**, *14* (3), 1603–1608. https://doi.org/10.1021/nl500037x.

(55) Zheng, Z.; Ng, Y. H.; Wang, D. W.; Amal, R. Epitaxial Growth of Au–Pt–Ni Nanorods for Direct High Selectivity H2O2Production. *Adv. Mater.* **2016**, *28* (45), 9949–9955. https://doi.org/10.1002/adma.201603662.

(56) Dai, L. Functionalization of Graphene for Efficient Energy Conversion and Storage. *Acc. Chem. Res.* **2013**, *46* (1), 31–42. https://doi.org/10.1021/ar300122m.

(57) Liu, J.; Song, P.; Ning, Z.; Xu, W. Recent Advances in Heteroatom-Doped Metal-Free Electrocatalysts for Highly Efficient Oxygen Reduction Reaction. *Electrocatalysis* **2015**, *6* (2), 132–147. https://doi.org/10.1007/s12678-014-0243-9.

(58) Wong, W. Y.; Daud, W. R. W.; Mohamad, A. B.; Kadhum, A. A. H.; Loh, K. S.; Majlan, E. H. Recent Progress in Nitrogen-Doped Carbon and Its Composites as Electrocatalysts for Fuel Cell Applications. *Int. J. Hydrogen Energy* **2013**, *38* (22), 9370–9386.

https://doi.org/10.1016/j.ijhydene.2012.12.095.

(59) Terrones, H.; Lv, R.; Terrones, M.; Dresselhaus, M. S. The Role of Defects and Doping in 2D Graphene Sheets and 1D Nanoribbons. *Rep. Prog. Phys.* **2012**, *75* (6), 062501. https://doi.org/10.1088/0034-4885/75/6/062501.

(60) Kim, H. W.; Ross, M. B.; Kornienko, N.; Zhang, L.; Guo, J.; Yang, P.; McCloskey, B. D. Efficient Hydrogen Peroxide Generation Using Reduced Graphene Oxide-Based Oxygen Reduction Electrocatalysts. *Nat. Catal.* **2018**, *1* (4), 282–290. https://doi.org/10.1038/s41929-018-0044-2.

(61) Han, L.; Sun, Y.; Li, S.; Cheng, C.; Halbig, C. E.; Feicht, P.; Hübner, J. L.; Strasser, P.; Eigler, S. In-Plane Carbon Lattice-Defect Regulating Electrochemical Oxygen Reduction to Hydrogen Peroxide Production over Nitrogen-Doped Graphene. *ACS Catal.* **2019**, *9* (2), 1283–1288. https://doi.org/10.1021/acscatal.8b03734.

(62) Iglesias, D.; Giuliani, A.; Melchionna, M.; Marchesan, S.; Criado, A.; Nasi, L.; Bevilacqua, M.; Tavagnacco, C.; Vizza, F.; Prato, M.; Fornasiero, P. N-Doped Graphitized Carbon Nanohorns as a Forefront Electrocatalyst in Highly Selective O2 Reduction to H2O2. *Chem* **2018**, *4* (1), 106–123. https://doi.org/10.1016/j.chempr.2017.10.013.

(63) Sun, Y.; Li, S.; Jovanov, Z. P.; Bernsmeier, D.; Wang, H.; Paul, B.; Wang, X.; Kühl, S.; Strasser, P. Structure, Activity, and Faradaic Efficiency of Nitrogen-Doped Porous Carbon Catalysts for Direct Electrochemical Hydrogen Peroxide Production. *ChemSusChem* **2018**, *11* (19), 3388–3395. https://doi.org/10.1002/cssc.201801583.

(64) Sun, Y.; Sinev, I.; Ju, W.; Bergmann, A.; Dresp, S.; Kühl, S.; Spöri, C.; Schmies, H.; Wang, H.; Bernsmeier, D.; Paul, B.; Schmack, R.; Kraehnert, R.; Roldan Cuenya, B.; Strasser, P. Efficient Electrochemical Hydrogen Peroxide Production from Molecular Oxygen on Nitrogen-Doped Mesoporous Carbon Catalysts. *ACS Catal.* **2018**, *8* (4), 2844–2856. https://doi.org/10.1021/acscatal.7b03464.

(65) Sun, Y.; Silvioli, L.; Sahraie, N. R.; Ju, W.; Li, J.; Zitolo, A.; Li, S.; Bagger, A.; Arnarson, L.; Wang, X.; Moeller, T.; Bernsmeier, D.; Rossmeisl, J.; Jaouen, F.; Strasser, P. Activity–Selectivity Trends in the Electrochemical Production of Hydrogen Peroxide over Single-Site Metal–Nitrogen–Carbon Catalysts. *J. Am. Chem. Soc.* **2019**, *141* (31), 12372–12381.

https://doi.org/10.1021/jacs.9b05576.

(66) Melchionna, M.; Fornasiero, P.; Prato, M. The Rise of Hydrogen Peroxide as the Main Product by Metal-Free Catalysis in Oxygen Reductions. *Adv. Mater.* **2019**, *31* (13), 1–5. https://doi.org/10.1002/adma.201802920.

(67) Kim, J. H.; Kim, Y. T.; Joo, S. H. Electrocatalyst Design for Promoting Two-Electron Oxygen Reduction Reaction: Isolation of Active Site Atoms. *Current Opinion in Electrochemistry*. Elsevier B.V. June 1, 2020, pp 109–116. https://doi.org/10.1016/j.coelec.2020.01.007.

(68) Liu, Y.; Quan, X.; Fan, X.; Wang, H.; Chen, S. High-Yield Electrosynthesis of Hydrogen Peroxide from Oxygen Reduction by Hierarchically Porous Carbon. *Angew. Chemie* **2015**, *127* (23), 6941–6945. https://doi.org/10.1002/ange.201502396.

(69) Yang, W.; Zhou, M.; Cai, J.; Liang, L.; Ren, G.; Jiang, L. Ultrahigh Yield of Hydrogen Peroxide on Graphite Felt Cathode Modified with Electrochemically Exfoliated Graphene. *J. Mater. Chem. A* **2017**, *5* (17), 8070–8080. https://doi.org/10.1039/C7TA01534H.

(70) Zhang, L.; Xu, Q.; Niu, J.; Xia, Z. Role of Lattice Defects in Catalytic Activities of Graphene Clusters for Fuel Cells. *Phys. Chem. Chem. Phys.* **2015**, *17* (26), 16733–16743. https://doi.org/10.1039/c5cp02014j.

(71) Yan, X.; Jia, Y.; Yao, X. Defects on Carbons for Electrocatalytic Oxygen Reduction. *Chem. Soc. Rev.* **2018**, *47* (20), 7628–7658. https://doi.org/10.1039/c7cs00690j.

(72) Jiang, S.; Li, Z.; Wang, H.; Wang, Y.; Meng, L.; Song, S. Tuning Nondoped Carbon Nanotubes to an Efficient Metal-Free Electrocatalyst for Oxygen Reduction Reaction by Localizing the Orbital of the Nanotubes with Topological Defects. *Nanoscale* **2014**, *6* (23), 14262–14269. https://doi.org/10.1039/c4nr04658g.

(73) Pan, Z.; Wang, K.; Wang, Y.; Tsiakaras, P.; Song, S. In-Situ Electrosynthesis of Hydrogen Peroxide and Wastewater Treatment Application: A Novel Strategy for Graphite Felt Activation. *Appl. Catal. B Environ.* **2018**, *237* (May), 392–400. https://doi.org/10.1016/j.apcatb.2018.05.079.

(74) Chai, G.-L.; Hou, Z.; Ikeda, T.; Terakura, K. Two-Electron Oxygen Reduction on Carbon Materials Catalysts: Mechanisms and Active Sites. *J. Phys. Chem. C* **2017**, *121* (27), 14524–14533. https://doi.org/10.1021/acs.jpcc.7b04959.

(75) Jiang, Y.; Yang, L.; Sun, T.; Zhao, J.; Lyu, Z.; Zhuo, O.; Wang, X.; Wu, Q.; Ma, J.; Hu, Z. Significant Contribution of Intrinsic Carbon Defects to Oxygen Reduction Activity. *ACS Catal.* **2015**, *5* (11), 6707–6712. https://doi.org/10.1021/acscatal.5b01835.

(76) Oubal, M.; Picaud, S.; Rayez, M. T.; Rayez, J. C. Adsorption of Atmospheric Oxidants at Divacancy Sites of Graphene: A DFT Study. *Comput. Theor. Chem.* **2013**, *1016*, 22–27. https://doi.org/10.1016/j.comptc.2013.04.017.

(77) Han, G.-F.; Li, F.; Zou, W.; Karamad, M.; Jeon, J.-P.; Kim, S.-W.; Kim, S.-J.; Bu, Y.; Fu, Z.; Lu, Y.; Siahrostami, S.; Baek, J.-B. Building and Identifying Highly Active Oxygenated Groups in Carbon Materials for Oxygen Reduction to H2O2. *Nat. Commun.* **2020**, *11* (1), 2209. https://doi.org/10.1038/s41467-020-15782-z.

(78) Peng, Y.; Lu, B.; Chen, S. Carbon-Supported Single Atom Catalysts for Electrochemical Energy Conversion and Storage. *Adv. Mater.* **2018**, *30* (48), 1–25. https://doi.org/10.1002/adma.201801995.

(79) Gawande, M. B.; Fornasiero, P.; Zbořil, R. Carbon-Based Single-Atom Catalysts for Advanced Applications. *ACS Catal.* **2020**, *10* (3), 2231–2259. https://doi.org/10.1021/acscatal.9b04217.

(80) Gao, J.; Yang, H. bin; Huang, X.; Hung, S. F.; Cai, W.; Jia, C.; Miao, S.; Chen, H. M.; Yang, X.; Huang, Y.; Zhang, T.; Liu, B. Enabling Direct H2O2 Production in Acidic Media through Rational Design of Transition Metal Single Atom Catalyst. *Chem* **2020**, *6* (3), 658–674. https://doi.org/10.1016/j.chempr.2019.12.008.

(81) Li, B. Q.; Zhao, C. X.; Liu, J. N.; Zhang, Q. Electrosynthesis of Hydrogen Peroxide Synergistically Catalyzed by Atomic Co–Nx–C Sites and Oxygen Functional Groups in Noble-Metal-Free Electrocatalysts. *Adv. Mater.* **2019**, *31* (35), 1–8. https://doi.org/10.1002/adma.201808173.

(82) Siahrostami, S.; Björketun, M. E.; Strasser, P.; Greeley, J.; Rossmeisl, J. Tandem Cathode for Proton Exchange Membrane Fuel Cells. *Phys. Chem. Chem. Phys.* **2013**, *15* (23), 9326–9334. https://doi.org/10.1039/c3cp51479j.

(83) Tang, C.; Jiao, Y.; Shi, B.; Liu, J. N.; Xie, Z.; Chen, X.; Zhang, Q.; Qiao, S. Z. Coordination Tunes Selectivity: Two-Electron Oxygen Reduction on High-Loading Molybdenum Single-

Atom Catalysts. *Angew. Chemie - Int. Ed.* **2020**, 2–8. https://doi.org/10.1002/anie.202003842.

(84) Shen, R.; Chen, W.; Peng, Q.; Lu, S.; Zheng, L.; Cao, X.; Wang, Y.; Zhu, W.; Zhang, J.; Zhuang, Z.; Chen, C.; Wang, D.; Li, Y. High-Concentration Single Atomic Pt Sites on Hollow CuSx for Selective O2 Reduction to H2O2 in Acid Solution. *Chem* **2019**, *5* (8), 2099–2110. https://doi.org/https://doi.org/10.1016/j.chempr.2019.04.024.

(85) Lenarda, A.; Bevilacqua, M.; Tavagnacco, C.; Nasi, L.; Criado, A.; Vizza, F.; Melchionna, M.; Prato, M.; Fornasiero, P. Selective Electrocatalytic H 2 O 2 Generation by Cobalt@N-Doped Graphitic Carbon Core–Shell Nanohybrids. *ChemSusChem* **2019**, *12* (8), 1664–1672. https://doi.org/10.1002/cssc.201900238.

(86) Gan, J.; Luo, W.; Chen, W.; Guo, J.; Xiang, Z.; Chen, B.; Yang, F.; Cao, Y.; Song, F.; Duan, X.; Zhou, X. Mechanistic Understanding of Size-Dependent Oxygen Reduction Activity and Selectivity over Pt/CNT Nanocatalysts. *Eur. J. Inorg. Chem.* **2019**, *2019* (27), 3210–3217. https://doi.org/10.1002/ejic.201801521.

(87) Kim, J. H.; Shin, D.; Lee, J.; Baek, D. S.; Shin, T. J.; Kim, Y.-T.; Jeong, H. Y.; Kwak, J. H.; Kim, H.; Joo, S. H. A General Strategy to Atomically Dispersed Precious Metal Catalysts for Unravelling Their Catalytic Trends for Oxygen Reduction Reaction. *ACS Nano* **2020**, *14*, 1990. https://doi.org/10.1021/acsnano.9b08494.

(88) Jung, E.; Shin, H.; Lee, B.-H.; Efremov, V.; Lee, S.; Lee, H. S.; Kim, J.; Hooch Antink, W.; Park, S.; Lee, K.-S.; Cho, S.-P.; Yoo, J. S.; Sung, Y.-E.; Hyeon, T. Atomic-Level Tuning of Co–N–C Catalyst for High-Performance Electrochemical H2O2 Production. *Nat. Mater.* **2020**. https://doi.org/10.1038/s41563-019-0571-5.

(89) Wong, C. H. A.; Sofer, Z.; Kube ova, M.; Ku era, J.; Mat jkova, S.; Pumera, M. Synthetic Routes Contaminate Graphene Materials with a Whole Spectrum of Unanticipated Metallic Elements. *Proc. Natl. Acad. Sci.* **2014**, *111* (38), 13774–13779. https://doi.org/10.1073/pnas.1413389111.

(90) Wu, Y.; Muthukrishnan, A.; Nagata, S.; Nabae, Y. Kinetic Understanding of the Reduction of Oxygen to Hydrogen Peroxide over an N-Doped Carbon Electrocatalyst. *J. Phys. Chem. C* **2019**, *123* (7), 4590–4596. https://doi.org/10.1021/acs.jpcc.8b12464.

(91) Wang, H.; Maiyalagan, T.; Wang, X. Review on Recent Progress in Nitrogen-Doped Graphene: Synthesis, Characterization, and Its Potential Applications. *ACS Catal.* **2012**, *2* (5), 781–794. https://doi.org/10.1021/cs200652y.

(92) Chen, G.; Liu, J.; Li, Q.; Guan, P.; Yu, X.; Xing, L.; Zhang, J.; Che, R. A Direct H2O2 Production Based on Hollow Porous Carbon Sphere-Sulfur Nanocrystal Composites by Confinement Effect as Oxygen Reduction Electrocatalysts. *Nano Res.* **2019**, *12* (10), 2614–2622. https://doi.org/10.1007/s12274-019-2496-3.

(93) Zhao, K.; Su, Y.; Quan, X.; YM, L.; Chen, S.; HT, Y. Enhanced H2O2 Production by Selective Electrochemical Reduction of O-2 on Fluorine-Doped Hierarchically Porous Carbon. *J. Catal.* **2018**, *357*, 118–126. https://doi.org/10.1016/j.jcat.2017.11.008.

(94) Q. Chang, P. Zhang, A. H. Bagherzadeh Mostaghimi, X. Zhao, S. R. Denny, J. Hoon Lee, H. Gao, Y. Zhang, H. Xin, S. Siahrostami, J. G. Chen, Z. C. Promoting H2O2 Production via 2-Electron Oxygen Reduction in Acidic Electrolyte by Coordinating Partially Oxidized Pd with Defect Carbon. *Nat. Commun.* **2020**.

(95) Wang, T.; Zeng, Z.; Cao, L.; Li, Z.; Hu, X.; An, B.; Wang, C.; Lin, W. A Dynamically Stabilized Single-Nickel Electrocatalyst for Selective Reduction of Oxygen to Hydrogen Peroxide. *Chem. - A Eur. J.* **2018**, *24* (64), 17011–17018. https://doi.org/10.1002/chem.201804312.

(96) Yin, X.; Lin, L.; Martinez, U.; Zelenay, P. 2,2'-Dipyridylamine as Heterogeneous Organic Molecular Electrocatalyst for Two-Electron Oxygen Reduction Reaction in Acid Media. *ACS Appl. Energy Mater.* **2019**, *2* (10), 7272–7278. https://doi.org/10.1021/acsaem.9b01227.

(97) Burke, M. S.; Enman, L. J.; Batchellor, A. S.; Zou, S.; Boettcher, S. W. Oxygen Evolution Reaction Electrocatalysis on Transition Metal Oxides and (Oxy)Hydroxides: Activity Trends and Design Principles. *Chem. Mater.* **2015**, *27* (22), 7549–7558. https://doi.org/10.1021/acs.chemmater.5b03148.

(98) Friebel, D.; Louie, M. W.; Bajdich, M.; Sanwald, K. E.; Cai, Y.; Wise, A. M.; Cheng, M.-J.; Sokaras, D.; Weng, T.-C.; Alonso-Mori, R.; Davis, R. C.; Bargar, J. R.; Nørskov, J. K.; Nilsson, A.; Bell, A. T. Identification of Highly Active Fe Sites in (Ni,Fe)OOH for Electrocatalytic Water Splitting. *J. Am. Chem. Soc.* **2015**, *137* (3), 1305–1313.

https://doi.org/10.1021/ja511559d.

(99) Chen, D.; Fang, Y.-H.; Liu, Z.-P. Searching for Active Binary Rutile Oxide Catalyst for Water Splitting from First Principles. *Phys. Chem. Chem. Phys.* **2012**, *14* (48), 16612–16617. https://doi.org/10.1039/c2cp42149f.

(100) Zhang, B.; Zheng, X.; Voznyy, O.; Comin, R.; Bajdich, M.; García-Melchor, M.; Han, L.; Xu, J.; Liu, M.; Zheng, L.; García de Arquer, F. P.; Dinh, C. T.; Fan, F.; Yuan, M.; Yassitepe, E.; Chen, N.; Regier, T.; Liu, P.; et al. Homogeneously Dispersed, Multimetal Oxygen-Evolving Catalysts. *Science* **2016**, aaf1525. https://doi.org/10.1126/science.aaf1525.

(101) Reier, T.; Oezaslan, M.; Strasser, P. Electrocatalytic Oxygen Evolution Reaction (OER) on Ru, Ir, and Pt Catalysts: A Comparative Study of Nanoparticles and Bulk Materials. *ACS Catal.* **2012**, *2* (8), 1765–1772. https://doi.org/10.1021/cs3003098.

(102) Fabbri, E.; Habereder, A.; Waltar, K.; Kötz, R.; Schmidt, T. J. Developments and Perspectives of Oxide-Based Catalysts for the Oxygen Evolution Reaction. *Catal. Sci. Technol.* **2014**, *4* (11), 3800–3821. https://doi.org/10.1039/C4CY00669K.

(103) Gong, M.; Dai, H. A Mini Review of NiFe-Based Materials as Highly Active Oxygen Evolution Reaction Electrocatalysts. *Nano Res.* **2014**, *8* (1), 23–39. https://doi.org/10.1007/s12274-014-0591-z.

(104) Cheng, Y.; Jiang, S. P. Advances in Electrocatalysts for Oxygen Evolution Reaction of Water Electrolysis-from Metal Oxides to Carbon Nanotubes. *Prog. Nat. Sci. Mater. Int.* **2015**, *25* (6), 545–553. https://doi.org/10.1016/j.pnsc.2015.11.008.

(105) Diaz-Morales, O.; Ledezma-Yanez, I.; Koper, M. T. M.; Calle-Vallejo, F. Guidelines for the Rational Design of Ni-Based Double Hydroxide Electrocatalysts for the Oxygen Evolution Reaction. *ACS Catal.* **2015**, *5* (9), 5380–5387. https://doi.org/10.1021/acscatal.5b01638.

(106) Izgorodin, A.; Izgorodina, E.; MacFarlane, D. R. Low Overpotential Water Oxidation to Hydrogen Peroxide on a MnOx Catalyst. *Energy Environ. Sci.* **2012**, *5* (11), 9496. https://doi.org/10.1039/c2ee21832a.

(107) McDonnell-Worth, C.; MacFarlane, D. R. Ion Effects in Water Oxidation to Hydrogen Peroxide. *RSC Adv.* **2014**, *4* (58), 30551. https://doi.org/10.1039/C4RA05296J.

(108) GOTO, H. Quantitative Analysis of Superoxide Ion and Hydrogen Peroxide Produced from

Molecular Oxygen on Photoirradiated TiO2 Particles. *J. Catal.* **2004**, *225* (1), 223–229. https://doi.org/10.1016/j.jcat.2004.04.001.

(109) Hirakawa, T.; Yawata, K.; Nosaka, Y. Photocatalytic Reactivity for O2− and OH Radical Formation in Anatase and Rutile TiO2 Suspension as the Effect of H2O2 Addition. *Appl. Catal. A Gen.* **2007**, *325* (1), 105–111. https://doi.org/10.1016/j.apcata.2007.03.015.

(110) Cai, R.; Kubota, Y.; Fujishima, A. Effect of Copper Ions on the Formation of Hydrogen Peroxide from Photocatalytic Titanium Dioxide Particles. *J. Catal.* **2003**, *219* (1), 214–218. https://doi.org/10.1016/S0021-9517(03)00197-0.

(111) Zhang, J.; Nosaka, Y. Quantitative Detection of OH Radicals for Investigating the Reaction Mechanism of Various Visible-Light TiO 2 Photocatalysts in Aqueous Suspension. *J. Phys. Chem. C* **2013**, *117* (3), 1383–1391. https://doi.org/10.1021/jp3105166.

(112) Sánchez-Quiles, D.; Tovar-Sánchez, A. Sunscreens as a Source of Hydrogen Peroxide Production in Coastal Waters. *Environ. Sci. Technol.* **2014**, *48* (16), 9037–9042. https://doi.org/10.1021/es5020696.

(113) Park, H. S.; Leonard, K. C.; Bard, A. J. Surface Interrogation Scanning Electrochemical Microscopy (SI-SECM) of Photoelectrochemistry at a W/Mo-BiVO 4 Semiconductor Electrode: Quantification of Hydroxyl Radicals during Water Oxidation. *J. Phys. Chem. C* **2013**, *117* (23), 12093–12102. https://doi.org/10.1021/jp400478z.

(114) Saison, T.; Chemin, N.; Chanéac, C.; Durupthy, O.; Mariey, L.; Maugé, F.; Brezová, V.; Jolivet, J.-P. New Insights Into BiVO 4 Properties as Visible Light Photocatalyst. *J. Phys. Chem. C* **2015**, *119* (23), 12967–12977. https://doi.org/10.1021/acs.jpcc.5b01468.

(115) Rettie, A. J. E.; Lee, H. C.; Marshall, L. G.; Lin, J.-F.; Capan, C.; Lindemuth, J.; McCloy, J. S.; Zhou, J.; Bard, A. J.; Mullins, C. B. Combined Charge Carrier Transport and Photoelectrochemical Characterization of BiVO4 Single Crystals: Intrinsic Behavior of a Complex Metal Oxide. *J. Am. Chem. Soc.* **2013**, *135* (30), 11389–11396. https://doi.org/10.1021/ja405550k.

(116) Nishikawa, M.; Hiura, S.; Mitani, Y.; Nosaka, Y. Enhanced Photocatalytic Activity of BiVO4 by Co-Grafting of Metal Ions and Combining with CuBi2O4. *J. Photochem. Photobiol. A Chem.* **2013**, *262*, 52–56. https://doi.org/10.1016/j.jphotochem.2013.04.018.

(117) Fuku, K.; Sayama, K. Efficient Oxidative Hydrogen Peroxide Production and Accumulation in Photoelectrochemical Water Splitting Using a Tungsten Trioxide/Bismuth Vanadate Photoanode. *Chem. Commun. (Camb).* **2016**, *52* (31), 5406–5409. https://doi.org/10.1039/c6cc01605g.

(118) Viswanathan, V.; Hansen, H. A.; Nørskov, J. K. Selective Electrochemical Generation of Hydrogen Peroxide from Water Oxidation. *J. Phys. Chem. Lett.* **2015**, *6* (21), 4224–4228. https://doi.org/10.1021/acs.jpclett.5b02178.

(119) Siahrostami, S.; Li, G.-L.; Viswanathan, V.; Nørskov, J. K. One- or Two-Electron Water Oxidation, Hydroxyl Radical, or H_2O_2 Evolution. *J. Phys. Chem. Lett.* **2017**, *8* (6), 1157–1160. https://doi.org/10.1021/acs.jpclett.6b02924.

(120) Man, I. C.; Su, H.-Y.; Calle-Vallejo, F.; Hansen, H. A.; Martínez, J. I.; Inoglu, N. G.; Kitchin, J.; Jaramillo, T. F.; Nørskov, J. K.; Rossmeisl, J. Universality in Oxygen Evolution Electrocatalysis on Oxide Surfaces. *ChemCatChem* **2011**, *3* (7), 1159–1165. https://doi.org/10.1002/cctc.201000397.

(121) Fernández, E. M.; Moses, P. G.; Toftelund, A.; Hansen, H. A.; Martínez, J. I.; Abild-Pedersen, F.; Kleis, J.; Hinnemann, B.; Rossmeisl, J.; Bligaard, T.; Nørskov, J. K. Scaling Relationships for Adsorption Energies on Transition Metal Oxide, Sulfide, and Nitride Surfaces. *Angew. Chem. Int. Ed. Engl.* **2008**, *47* (25), 4683–4686. https://doi.org/10.1002/anie.200705739.

(122) Bard, Allen J., Parsons Roger, Hordan, J. *Standard Potentials in Aqueous Solution*, 1st ed.; Bard, Allen J., Parsons Roger, Hordan, J., Ed.; M. Dekker: New York, 1985.

(123) Siahrostami, S.; Björketun, M. E.; Strasser, P.; Greeley, J.; Rossmeisl, J. Tandem Cathode for Proton Exchange Membrane Fuel Cells. *Phys. Chem. Chem. Phys.* **2013**, *15* (23), 9326–9334. https://doi.org/10.1039/c3cp51479j.

(124) Montoya, J. H.; Garcia-Mota, M.; Nørskov, J. K.; Vojvodic, A. Theoretical Evaluation of the Surface Electrochemistry of Perovskites with Promising Photon Absorption Properties for Solar Water Splitting. *Phys. Chem. Chem. Phys.* **2015**, *17* (4), 2634–2640. https://doi.org/10.1039/c4cp05259e.

(125) Siahrostami, S.; Li, G.-L.; Viswanathan, V.; Nørskov, J. K. One- or Two-Electron Water

Oxidation, Hydroxyl Radical, or H_2O_2 Evolution. *J. Phys. Chem. Lett.* **2017**, 1157–1160. https://doi.org/10.1021/acs.jpclett.6b02924.

(126) Hansen, H. A.; Viswanathan, V.; Nørskov, J. K. Unifying Kinetic and Thermodynamic Analysis of 2 e^- and 4 e^- Reduction of Oxygen on Metal Surfaces. *J. Phys. Chem. C* **2014**, *118* (13), 6706–6718. https://doi.org/10.1021/jp4100608.

(127) Montoya, J. H.; Doyle, A. D.; Nørskov, J. K.; Vojvodic, A. Trends in Adsorption of Electrocatalytic Water Splitting Intermediates on Cubic ABO3 Oxides. *Phys. Chem. Chem. Phys.* **2018**, *20* (5), 3813–3818. https://doi.org/10.1039/C7CP06539F.

(128) Persson, K. A.; Waldwick, B.; Lazic, P.; Ceder, G. Prediction of Solid-Aqueous Equilibria: Scheme to Combine First-Principles Calculations of Solids with Experimental Aqueous States. *Phys. Rev. B* **2012**, *85* (23), 235438. https://doi.org/10.1103/PhysRevB.85.235438.

(129) Jain, A.; Ong, S. P.; Hautier, G.; Chen, W.; Richards, W. D.; Dacek, S.; Cholia, S.; Gunter, D.; Skinner, D.; Ceder, G.; Persson, K. A. Commentary: The Materials Project: A Materials Genome Approach to Accelerating Materials Innovation. *APL Mater.* **2013**, *1* (1). https://doi.org/10.1063/1.4812323.

(130) Toma, F. M.; Cooper, J. K.; Kunzelmann, V.; McDowell, M. T.; Yu, J.; Larson, D. M.; Borys, N. J.; Abelyan, C.; Beeman, J. W.; Yu, K. M.; Yang, J.; Chen, L.; Shaner, M. R.; Spurgeon, J.; Houle, F. A.; Persson, K. A.; Sharp, I. D. Mechanistic Insights into Chemical and Photochemical Transformations of Bismuth Vanadate Photoanodes. *Nat. Commun.* **2016**, *7*, 12012.

(131) Ong, S. P.; Richards, W. D.; Jain, A.; Hautier, G.; Kocher, M.; Cholia, S.; Gunter, D.; Chevrier, V. L.; Persson, K. A.; Ceder, G. Python Materials Genomics (Pymatgen): A Robust, Open-Source Python Library for Materials Analysis. *Comput. Mater. Sci.* **2013**, *68*, 314–319. https://doi.org/10.1016/j.commatsci.2012.10.028.

(132) Singh, A. K.; Zhou, L.; Shinde, A.; Suram, S. K.; Montoya, J. H.; Winston, D.; Gregoire, J. M.; Persson, K. A. Electrochemical Stability of Metastable Materials. *Chem. Mater.* **2017**, *29* (23), 10159–10167. https://doi.org/10.1021/acs.chemmater.7b03980.

(133) Patel, A. M.; Nørskov, J. K.; Persson, K. A.; Montoya, J. H. Efficient Pourbaix Diagrams of Many-Element Compounds. *Phys. Chem. Chem. Phys.* **2019**, *21* (45), 25323–25327.

https://doi.org/10.1039/C9CP04799A.

(134) Xia, C.; Xia, Y.; Zhu, P.; Fan, L.; Wang, H. Direct Electrosynthesis of Pure Aqueous H2O2solutions up to 20% by Weight Using a Solid Electrolyte. *Science (80-.).* **2019**, *366* (6462), 226–231. https://doi.org/10.1126/science.aay1844.

(135) Zhang, H.; Zhao, Y.; Li, Y.; Li, G.; Li, J.; Zhang, F. Janus Electrode of Asymmetric Wettability for H2O2 Production with Highly Efficient O2 Utilization. *ACS Appl. Energy Mater.* **2020**, *3* (1), 705–714. https://doi.org/10.1021/acsaem.9b01908.

(136) Zhu, Q.; Pan, Z.; Hu, S.; Kim, J.-H. Cathodic Hydrogen Peroxide Electrosynthesis Using Anthraquinone Modified Carbon Nitride on Gas Diffusion Electrode. *ACS Appl. Energy Mater.* **2019**, *2* (11), 7972–7979. https://doi.org/10.1021/acsaem.9b01445.

(137) Han, Z.; Horak, K. T.; Lee, H. B.; Agapie, T. Tetranuclear Manganese Models of the OEC Displaying Hydrogen Bonding Interactions: Application to Electrocatalytic Water Oxidation to Hydrogen Peroxide. *J. Am. Chem. Soc.* **2017**, *139* (27), 9108–9111. https://doi.org/10.1021/jacs.7b03044.

TOC

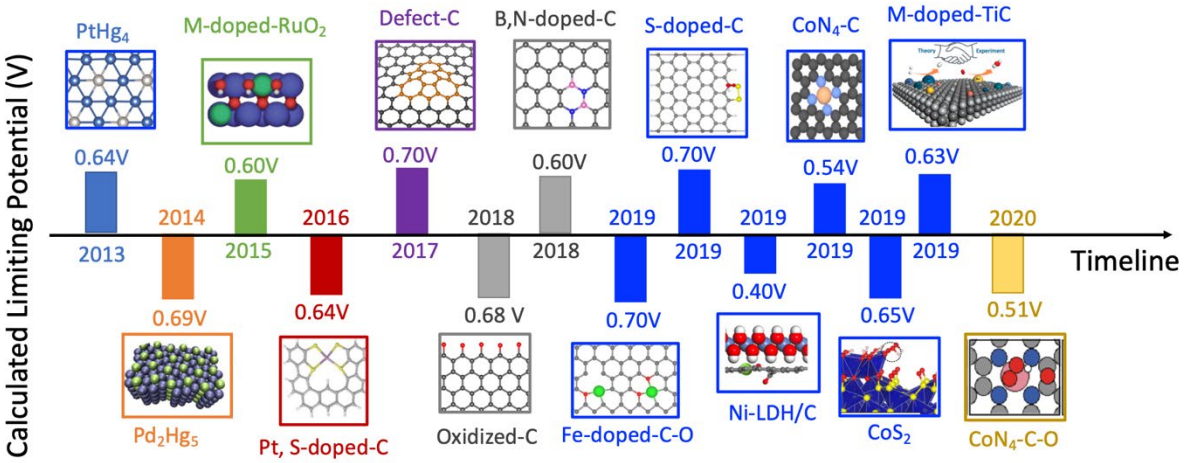
Calculated Limiting Potential (V)
PtHg4
0.64V
2013
Pd2Hg5
0.69V
2014
M-doped-RuO2
0.60V
2015
Pt, S-doped-C
0.64V
2016
Defect-C
0.70V
2017
Oxidized-C
0.68 V
2018
B,N-doped-C
0.60V
2018
Fe-doped-C-O
0.70V
2019
S-doped-C
0.70V
2019
Ni-LDH/C
0.40V
2019
CoN4-C
0.54V
2019
CoS2
0.65V
2019
M-doped-TiC
0.63V
2019
CoN4-C-O
0.51V
2020
Timeline